

The Scalar Triplet Contribution to Lepton Flavour Violation and Neutrinoless Double Beta Decay in Left-Right Symmetric Model

Gulab Bambhaniya,^a P. S. Bhupal Dev,^{b,c} Srubabati Goswami,^a and Manimala Mitra^d

^a*Physical Research Laboratory, Navrangpura, Ahmedabad 380009, India*

^b*Physik-Department T30d, Technische Universität München, James-Frank-Straße 1, D-85748 Garching, Germany*

^c*Max-Planck-Institut für Kernphysik, Saupfercheckweg 1, D-69117 Heidelberg, Germany*

^d*Indian Institute of Science Education and Research Mohali, Knowledge City, Sector 81, SAS Nagar, Manauli 140306, India*

E-mail: gulab@prl.res.in, bhupal.dev@mpi-hd.mpg.de, sruba@prl.res.in, manimala@iisermohali.ac.in

ABSTRACT: We analyse in detail the scalar triplet contribution to the low-energy lepton flavour violating (LFV) and lepton number violating (LNV) processes within a TeV-scale left-right symmetric framework. We show that in both type-I and type-II seesaw dominance for the light neutrino masses, the triplet of mass comparable to or smaller than the largest right-handed neutrino mass scale can give sizeable contribution to the LFV processes, except in the quasi-degenerate limit of light neutrino masses, where a suppression can occur due to cancellations. In particular, a moderate value of the heaviest neutrino to scalar triplet mass ratio $r \lesssim \mathcal{O}(1)$ is still experimentally allowed and can be explored in the future LFV experiments. Similarly, the contribution of a relatively light triplet to the LNV process of neutrinoless double beta decay could be significant, disfavouring a part of the model parameter space otherwise allowed by LFV constraints. Nevertheless, we find regions of parameter space consistent with both LFV and LNV searches, for which the values of the total effective neutrino mass can be accessible to the next generation ton-scale experiments. Such light triplets can also be directly searched for at the LHC, thus providing a complementary probe of this scenario. Finally, we also study the implications of the triplet contribution for the left-right symmetric model interpretation of the recent diboson anomaly at the LHC.

KEYWORDS: Left-Right Gauge Symmetry, Charged Higgs Bosons, Lepton Flavour Violation, Neutrinoless Double Beta Decay

Contents

1	Introduction	1
2	The model setup	2
3	Lepton flavour violation	5
4	Neutrinoless double beta decay	12
5	Diboson excess	17
6	Summary	19
	References	22

1 Introduction

The observation of nonzero neutrino masses and mixing provides the first unambiguous experimental evidence for physics beyond the Standard Model (SM) [1]. Although the origin of mass for all charged fermions in the SM seems to have been demystified by the Higgs boson discovery at the LHC [2, 3], the origin of tiny neutrino masses is still a nagging issue. A simple way to solve this puzzle is by breaking the global $B - L$ symmetry of the SM through Weinberg’s dimension-5 operator [4], whose tree-level realizations are the type-I [5–9], II [10–13] and III [14] seesaw mechanisms.

A natural renormalisable theory of the effective dimension-5 operator for the seesaw mechanism is the Left-Right (L-R) Symmetric Model (LRSM) of weak interactions, based on the gauge group $SU(2)_L \times SU(2)_R \times U(1)_{B-L}$ [15–18]. Here, the key ingredients of seesaw, namely, the right-handed (RH) neutrino fields, arise as the necessary parity gauge partner of the left-handed (LH) neutrino fields and are also required by anomaly cancellation, whereas the seesaw scale is identified as the one at which the RH counterpart of the SM $SU(2)_L$ gauge symmetry, namely the $SU(2)_R$ symmetry, is broken. The RH neutrinos acquire a Majorana mass as soon as the $SU(2)_R$ symmetry is spontaneously broken at a scale v_R , analogous to the way the SM charged fermions get masses when the $SU(2)_L$ symmetry is broken at the electroweak scale v . Thus, the Higgs field that gives mass to the RH neutrinos becomes the analogue of the 125 GeV Higgs boson discovered at the LHC.

The L-R symmetric theories lead to new effects or add new contributions to various new physics observables at both energy and intensity frontiers, which can be tested in current and future experiments, if the scale of parity restoration is below a few TeV. In particular, a TeV-scale LRSM leads to the spectacular lepton number violating (LNV) process of same-sign dilepton plus two jets at the LHC [19–27] (for reviews, see e.g. [28, 29]), as well

as potentially large contributions to its low-energy analogue, namely, neutrinoless double beta decay ($0\nu\beta\beta$) [6, 30–42]. In addition, there are a plethora of lepton flavour violating (LFV) processes, such as $\mu \rightarrow e\gamma$, $\mu \rightarrow 3e$, $\mu \rightarrow e$ conversion in nuclei, which can get sizeable contributions from the RH sector [23, 33–35, 37, 39, 42–49].

In this paper, we focus on the scalar triplet contribution to the low-energy LNV and LFV processes within a TeV-scale LRSM framework. It is known that for triplet masses much larger than the RH neutrino masses, its contributions to LNV and LFV processes are sub-dominant [33–35]. However, since the direct experimental searches for these triplets at the LHC still allow for the possibility of low triplet masses $\gtrsim 500$ GeV [50] and the current lower limits on the RH gauge boson masses are in the few TeV range [51–53], it is worthwhile analysing the possible scenarios where the triplet masses are comparable to or lower than the RH neutrino or RH gauge boson masses in the theory. In such cases, we find that the triplet contribution to $0\nu\beta\beta$ and LFV processes can indeed be sizeable. While for very large RH neutrino to Higgs triplet mass ratio, these contributions are already ruled out by existing experimental constraints, for moderate values of this mass ratio, there still exists some allowed parameter space which can be probed in future experiments. We emphasise that these low-energy searches are complementary to the direct probes of the scalar sector of the LRSM at colliders, where they lead to interesting multi-lepton signatures [54–64].

The rest of the paper is organised as follows: In Section 2, we review the basic features of the minimal LRSM. In Section 3, we discuss the LFV processes $\mu \rightarrow e\gamma$ and $\mu \rightarrow 3e$, and in Section 4, the predictions for $0\nu\beta\beta$ due to the triplet contributions. We discuss the implications for the diboson excess in Section 5. Our results are summarised in Section 6.

2 The model setup

The quarks and leptons are assigned to the following irreducible representations of the LRSM gauge group $SU(3)_c \times SU(2)_L \times SU(2)_R \times U(1)_{B-L}$ [15–18]:

$$\begin{aligned} Q_{L,i} &= \begin{pmatrix} u_L \\ d_L \end{pmatrix}_i : \left(\mathbf{3}, \mathbf{2}, \mathbf{1}, \frac{1}{3} \right), & Q_{R,i} &= \begin{pmatrix} u_R \\ d_R \end{pmatrix}_i : \left(\mathbf{3}, \mathbf{1}, \mathbf{2}, \frac{1}{3} \right), \\ \psi_{L,i} &= \begin{pmatrix} \nu_L \\ e_L \end{pmatrix}_i : (\mathbf{1}, \mathbf{2}, \mathbf{1}, -1), & \psi_{R,i} &= \begin{pmatrix} N_R \\ e_R \end{pmatrix}_i : (\mathbf{1}, \mathbf{1}, \mathbf{2}, -1), \end{aligned} \quad (2.1)$$

where $i = 1, 2, 3$ represents the family index, and the subscripts L, R denote the left and right-chiral projection operators $P_{L,R} = (1 \mp \gamma_5)/2$. For the scalar sector, the minimal model consists of the following representations:

$$\begin{aligned} \Phi &= \begin{pmatrix} \phi_1^0 & \phi_2^+ \\ \phi_1^- & \phi_2^0 \end{pmatrix} : (\mathbf{1}, \mathbf{2}, \mathbf{2}, 0), \\ \Delta_L &= \begin{pmatrix} \Delta_L^+/\sqrt{2} & \Delta_L^{++} \\ \Delta_L^0 & -\Delta_L^+/\sqrt{2} \end{pmatrix} : (\mathbf{1}, \mathbf{3}, \mathbf{1}, 2), \\ \Delta_R &= \begin{pmatrix} \Delta_R^+/\sqrt{2} & \Delta_R^{++} \\ \Delta_R^0 & -\Delta_R^+/\sqrt{2} \end{pmatrix} : (\mathbf{1}, \mathbf{1}, \mathbf{3}, 2). \end{aligned} \quad (2.2)$$

The gauge symmetry $SU(2)_R \times U(1)_{B-L}$ is broken down to the SM group $U(1)_Y$ by the vacuum expectation value (VEV) of the neutral component of the $SU(2)_R$ triplet Δ_R : $\langle \Delta_R^0 \rangle = v_R$.¹ This generates the Majorana masses of the RH neutrinos N_R , as well as the masses of the RH gauge bosons W_R and Z_R , and explains the small LH neutrino masses via the type-I seesaw mechanism [5–9]. The other Higgs triplet Δ_L acquires a small VEV $\langle \Delta_L^0 \rangle = v_L$ and contributes to the generation of light neutrino masses via the type-II seesaw mechanism [10–13]. The standard electroweak symmetry is broken by the VEV of the Higgs bi-doublet field Φ : $\langle \Phi \rangle = \text{diag}(\kappa_1, \kappa_2)$, which generates masses for the charged fermions, as well as the SM W and Z bosons. The mixing between the LH and RH gauge bosons is given by $\tan 2\xi \simeq 2\kappa_1\kappa_2/v_R^2$.

The current experimental constraints on the mass of the RH gauge boson $M_{W_R} \simeq g_R v_R / \sqrt{2} \gtrsim 3$ TeV (assuming the equality of the $SU(2)_L$ and $SU(2)_R$ gauge couplings, i.e. $g_L = g_R$) from direct LHC searches [51, 52], as well as from quark flavour changing neutral current (FCNC) processes [65–68], imply that $v_R \gtrsim 6$ TeV. Similarly, the constraints from the electroweak ρ -parameter [1] restrict $v_L \lesssim 2$ GeV. On the other hand, since the VEVs of the Φ field break the electroweak symmetry, we have $\kappa_1^2 + \kappa_2^2 = v^2$, where $v \simeq 174$ GeV is the electroweak VEV in the SM. Thus we expect to have the following hierarchy of VEVs:

$$v_L \ll \kappa_1, \kappa_2 \ll v_R. \quad (2.3)$$

Without loss of generality, we can choose κ_1 and v_R as real parameters, while κ_2 and v_L can, in general, be complex parameters.

The Yukawa Lagrangian in the lepton sector is given by

$$\begin{aligned}
-\mathcal{L}_Y &= h_{ij} \bar{\psi}_{L,i} \Phi \psi_{R,j} + \tilde{h}_{ij} \bar{\psi}_{L,i} \tilde{\Phi} \psi_{R,j} + f_{L,ij} \psi_{L,i}^T C i \tau_2 \Delta_L \psi_{L,j} \\
&\quad + f_{R,ij} \psi_{R,i}^T C i \tau_2 \Delta_R \psi_{R,j} + \text{H.c.},
\end{aligned} \quad (2.4)$$

where $C = i\gamma_2\gamma_0$ is the charge conjugation operator, $\tilde{\Phi} = \tau_2 \Phi^* \tau_2$, τ_2 is the second Pauli matrix and γ_μ are the Dirac matrices. After electroweak symmetry breaking, the Yukawa Lagrangian (2.4) leads to the following 6×6 neutrino mass matrix in the flavour basis,

$$\mathcal{M}_\nu = \begin{pmatrix} m_L & m_D \\ m_D^T & M_R \end{pmatrix}, \quad (2.5)$$

where the 3×3 Dirac and Majorana mass matrices are given by

$$m_D = \frac{1}{\sqrt{2}} (\kappa_1 h + \kappa_2 \tilde{h}), \quad m_L = \sqrt{2} v_L f_L, \quad M_R = \sqrt{2} v_R f_R. \quad (2.6)$$

In the seesaw approximation, using Eq. (2.3), the 3×3 light neutrino mass matrix can be written as

$$m_\nu \simeq m_L - m_D M_R^{-1} m_D^T = \sqrt{2} v_L f_L - \frac{\kappa^2}{\sqrt{2} v_R} h_D f_R^{-1} h_D^T, \quad (2.7)$$

¹In principle, the L-R symmetry can also be broken by a doublet Higgs field; however, in this case, the LH and RH neutrinos must necessarily pair up to form Dirac particles and do not give rise to the interesting LNV signals, such as $0\nu\beta\beta$ induced by neutrinos, as discussed here. Moreover, the decay $W_R \rightarrow \ell\nu_\ell$ would lead to an isolated lepton plus missing energy, and the null results at the LHC in this search channel would highly disfavour a TeV-scale W_R in the doublet-breaking scenario.

where $h_D \equiv (\kappa_1 h + \kappa_2 \tilde{h})/(\sqrt{2}\kappa)$ and $\kappa \equiv (|\kappa_1|^2 + |\kappa_2|^2)^{1/2}$.

We will do our analysis in two interesting limits of Eq. (2.7), which do not require any fine-tuning of the model parameters to get the observed light neutrino masses:

(i) Type-I dominance, where the VEV of Δ_L can be set to zero and the first term on the right-hand side of Eq. (2.7) vanishes, so that the light neutrino mass matrix is governed by the usual type-I seesaw contribution [6]:

$$m_\nu \simeq -m_D M_R^{-1} m_D^\top. \quad (2.8)$$

In this case, the light-heavy neutrino mixing $V_{\ell N} \simeq m_D M_R^{-1}$ may or may not give large contributions to the low-energy processes, depending on the textures of m_D and M_R as required to satisfy the neutrino oscillation data [39, 69]. Since our focus is on the triplet contribution, we will assume for simplicity that m_D is proportional to the identity matrix [34],² with the mixing $V_{\ell N} \lesssim 10^{-6}$, which satisfies the light neutrino mass constraint for TeV-scale M_R , without any fine-tuning. In this case, Eq. (2.8) suggests that $m_\nu \propto M_R^{-1}$ and the same PMNS mixing matrix U which diagonalises m_ν also diagonalises M_R^{-1} . This implies M_R is diagonalised by U^* , since U is assumed to be unitary. Moreover, the ratios of the RH neutrino mass eigenvalues (M_i) are related to the corresponding mass eigenvalues in the light neutrino sector (m_i), which are experimentally constrained for a given mass hierarchy. Thus, the only free parameter in the RH neutrino sector is the overall mass scale, which we will fix by specifying the heaviest neutrino mass eigenvalue, to be denoted hereafter by M_N . More explicitly, for normal hierarchy (NH) of light neutrino masses, we have $M_N = M_1$, and therefore, $M_2 = (m_1/m_2)M_N$ and $M_3 = (m_1/m_3)M_N$. Similarly, for inverted hierarchy (IH), we have $M_N = M_3$, and therefore, $M_1 = (m_3/m_1)M_N$ and $M_2 = (m_3/m_2)M_N$ [34].

(ii) Type-II dominance, when the Dirac mass term m_D is negligible, so that the light neutrino mass matrix is solely governed by the Higgs triplet contribution:

$$m_\nu \simeq m_L. \quad (2.9)$$

In this case, the light-heavy neutrino mixing $V_{\ell N}$ is necessarily small and does not play any role in the LNV and LFV observables. Moreover, if parity (or charge conjugation) is taken to be the discrete L-R symmetry at the TeV-scale, this implies $f_L = f_R$ (or $f_L = f_R^*$). Hence, Eq. (2.9) suggests that $m_\nu \propto M_R$, *i.e.*, the same PMNS mixing matrix U diagonalises both LH and RH neutrino sectors [33]. In this case, for NH, we have $M_N = M_3$, and therefore, $M_1 = (m_1/m_3)M_N$ and $M_2 = (m_2/m_3)M_N$, whereas for IH, we have $M_N = M_2$, and therefore, $M_1 = (m_1/m_2)M_N$ and $M_3 = (m_3/m_2)M_N$.

In the scalar sector of the minimal LRSM, there are 20 real degrees of freedom: 8 from the bi-doublet and 6 each from the LH and RH triplets. After spontaneous symmetry breaking, 6 of them are Goldstone bosons, which give masses to the LH and RH gauge bosons in both charged and neutral sectors. Thus, there remain 14 physical real scalar fields, one of which (h_ϕ^0) should be identified as the SM-like Higgs doublet with mass proportional to v , independent of the triplet VEVs. The remaining 13 scalar fields, *i.e.*,

²This could in principle be motivated from some flavour symmetry [70].

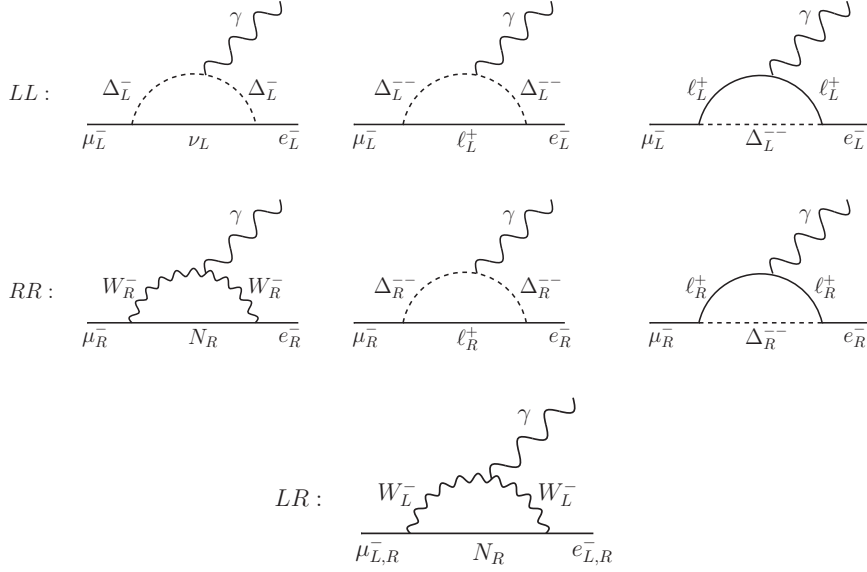


Figure 3.1: Feynman diagrams for $\mu \rightarrow e\gamma$ in the LRSM.

the doublets $H_\phi^0, A_\phi^0, H_\phi^\pm$, left triplets $H_L^0, A_L^0, \Delta_L^\pm, \Delta_L^{\pm\pm}$ and right triplets $H_R^0, \Delta_R^{\pm\pm}$ are all assumed to be heavy, since their masses are proportional to v_R [71]. In the following, we will be mostly interested in the masses of the doubly-charged scalars, and for simplicity, we will assume them to be equal in the LH and RH sectors. For convenience, we further define the parameter

$$\frac{1}{M_\Delta^2} = \frac{1}{m_{\Delta_L^{\pm\pm}}^2} + \frac{1}{m_{\Delta_R^{\pm\pm}}^2}, \quad (2.10)$$

and express our results for fixed values of the ratio of the heaviest neutrino mass M_N to M_Δ : $r \equiv M_N/M_\Delta$.

3 Lepton flavour violation

In the canonical SM seesaw, the LFV decay rates induced by the neutrino mixing are suppressed by the tiny neutrino masses, and hence, are well below the current experimental limits [72, 73] and even the distant-future sensitivities [74–76]. On the other hand, in the LRSM, several new contributions appear due to the additional RH current interactions, which could lead to sizeable LFV rates for a TeV-scale v_R . For example, the $\mu \rightarrow e\gamma$ process receives new contributions from both the scalar and gauge sectors, which can be classified into three categories, namely, those involving purely LH currents (LL), purely RH currents (RR) and mixed LH-RH currents (LR), as shown in Figure 3.1. The corresponding branching ratio is given by [35, 46]

$$\text{BR}(\mu \rightarrow e\gamma) = \frac{3\alpha_{\text{em}}}{2\pi} \left(|G_L^\gamma|^2 + |G_R^\gamma|^2 \right), \quad (3.1)$$

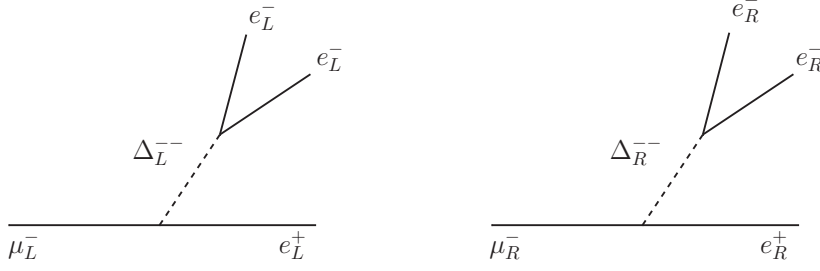


Figure 3.2: Feynman diagrams for $\mu \rightarrow 3e$ in the LRSM.

where $\alpha_{\text{em}} \equiv e^2/4\pi$ is the electromagnetic coupling constant, and the form factors G_R^γ and G_L^γ are given by

$$G_R^\gamma = \sum_{i=1}^3 \left(V_{\mu i} V_{ei}^* |\xi|^2 |G_1^\gamma(a_i)| - S_{\mu i}^* V_{ei}^* \xi e^{-i\alpha} G_2^\gamma(a_i) \frac{M_i}{m_\mu} + V_{\mu i} V_{ei}^* \left[\frac{m_{W_L}^2}{m_{W_R}^2} G_1^\gamma(b_i) + \frac{2b_i}{3} \frac{m_{W_L}^2}{m_{\Delta_R^{++}}^2} \right] \right), \quad (3.2)$$

$$G_L^\gamma = \sum_{i=1}^3 \left(S_{\mu i}^* S_{ei} G_1^\gamma(a_i) - V_{\mu i} S_{ei} \xi e^{i\alpha} G_2^\gamma(a_i) \frac{M_i}{m_\mu} + V_{\mu i} V_{ei}^* b_i \left[\frac{2}{3} \frac{m_{W_L}^2}{m_{\Delta_L^{++}}^2} + \frac{1}{12} \frac{m_{W_L}^2}{m_{\Delta_L^\pm}^2} \right] \right), \quad (3.3)$$

with $a_i \equiv (M_i/m_{W_L})^2$, $b_i \equiv (M_i/m_{W_R})^2$, α is the phase of the VEV κ_2 , m_μ is the muon mass, V is the RH neutrino mixing matrix which is related to the PMNS mixing matrix in our case, and S is the light-heavy neutrino mixing matrix which can be neglected for the choice of our parameters. Similarly, we can drop the terms depending on the $W_L - W_R$ mixing parameter ξ which is experimentally constrained to be $\lesssim 10^{-3}$ [1]. The loop functions $G_{1,2}^\gamma(a)$ are given as

$$G_1^\gamma(a) = -\frac{2a^3 + 5a^2 - a}{4(1-a)^3} - \frac{3a^3}{2(1-a)^4} \ln a, \quad (3.4)$$

$$G_2^\gamma(a) = \frac{a^2 - 11a + 4}{2(1-a)^2} - \frac{3a^2}{(1-a)^3} \ln a. \quad (3.5)$$

For the LFV process $\mu \rightarrow 3e$, the Higgs triplets Δ_L and Δ_R contribute at the tree level, as shown in Figure 3.2, thereby making the branching ratio of this process potentially large [46, 77–79]:

$$\text{BR}(\mu \rightarrow 3e) = \frac{1}{2} |h_{\mu e} h_{ee}^*|^2 \left(\frac{m_{W_L}^4}{m_{\Delta_L^{++}}^4} + \frac{m_{W_L}^4}{m_{\Delta_R^{++}}^4} \right), \quad (3.6)$$

where $h_{\alpha\beta} \equiv \sum_{i=1}^3 V_{\alpha i} V_{\beta i} M_i/m_{W_R}$. Note that there is also an one-loop induced contribution in the type-I dominance [80], which is however suppressed by the loop factors as well as by the light-heavy neutrino mixing, and hence, we can safely ignore it in our case, as compared to the tree-level contribution given by Eq. (3.6). In Ref. [33], it has been pointed

out that the current experimental constraint on $\text{BR}(\mu \rightarrow 3e) \leq 1.0 \times 10^{-12}$ [72] requires that in Eq. (3.6), the triplet scalar masses must be at least 10 times the heaviest RH neutrino mass scale in the theory, *i.e.*, the ratio $r \lesssim 0.1$, thereby making the Higgs triplet contribution to $\mu \rightarrow e\gamma$ and $0\nu\beta\beta$ negligible. We show that while this is true in general, there can be cancellations due to the variations of the so far unknown CP phases in the PMNS mixing matrix in which cases, this is not strictly required, *i.e.*, the $\mu \rightarrow 3e$ rate can in principle be compatible with the experimental constraint even for larger values of r . In these interesting scenarios, the Higgs triplet contribution to other LFV and $0\nu\beta\beta$ processes can become sizeable, and hence, must be included in the analysis. This is first illustrated with three representative values of r (moderate, small and large), where we show that r values as large as $\mathcal{O}(1)$ are still allowed by current experimental constraints, giving rise to interesting effects in low-energy LNV and LFV observables, as well as potential LNV signals at the LHC. Then we show the LFV-allowed parameter space as a function of the ratio r . We do not explicitly discuss here other interesting LFV processes, such as $\mu - e$ conversion in nuclei, or electric dipole moments, which are left for future studies.

Case-I: Moderate value of r

We first consider the scenario with $r = 0.707$. For illustration, we set the RH gauge boson mass $m_{W_R} = 3.5$ TeV, largest heavy neutrino mass $M_N = 500$ GeV and the Higgs triplet masses $M_{\text{scalar}} \equiv m_{\Delta_R^{++}} = m_{\Delta_L^{++}} = M_{\Delta_L^+} = 1$ TeV, which are consistent with the direct experimental constraints from the LHC. Using these parameters and Eqs. (3.1) and (3.6), we compute the $\mu \rightarrow e\gamma$ and $\mu \rightarrow 3e$ branching ratios, respectively, as a function of the lightest neutrino mass. We have taken into account the 3σ variation of the oscillation parameters as given by a recent global fit [81], as well as the variation of the Dirac CP phase δ between $[0, 2\pi]$ and Majorana phases $\alpha_{1,2}$ between $[0, \pi]$. We demand that our predicted LFV branching ratios should satisfy the current limits: $\text{BR}(\mu \rightarrow e\gamma) < 5.7 \times 10^{-13}$ from MEG [73] and $\text{BR}(\mu \rightarrow 3e) < 1.0 \times 10^{-12}$ from SINDRUM [72] experiments. Our results are shown in Figure 3.3 by the blue ($\mu \rightarrow e\gamma$) and red ($\mu \rightarrow 3e$) scattered points for normal hierarchy (NH, left panels) and inverted hierarchy (IH, right panels) in type-I (top panels) and type-II (bottom panels) dominance. We find that for the type-I, NH case, the predicted LFV branching ratios of $\mu \rightarrow e\gamma$ and $\mu \rightarrow 3e$ are allowed by the present experimental constraints, only if the lightest neutrino mass $m_1 \geq 0.01$ eV. For all other cases, lower values of $m_1(m_3)$ are allowed. A part of this parameter space with quasi-degenerate neutrinos is disfavoured by the most stringent limit on the sum of light neutrino masses $\sum_i m_i < 0.17$ eV at 95% C.L from Planck data [82], as shown by the green shaded region in Figure 3.3. We infer that for moderate values of r , the predicted LFV branching ratios for both type-I and type-II dominance are within the reach of future experiments, such as MEG-II [74], PRISM/PRIME [75] and Mu3e [76], as shown by the blue and red horizontal lines in Figure 3.3.

To better understand the dependence of the branching ratios on the lightest neutrino mass, next we consider only the best-fit values of the oscillation parameters, as depicted in Figures 3.4a and 3.4b, where we show the individual contributions G_L^γ, G_R^γ [*cf.* Eqs. (3.2) and (3.3)] to the branching ratio of $\mu \rightarrow e\gamma$, as well as the total contribution, for two dif-

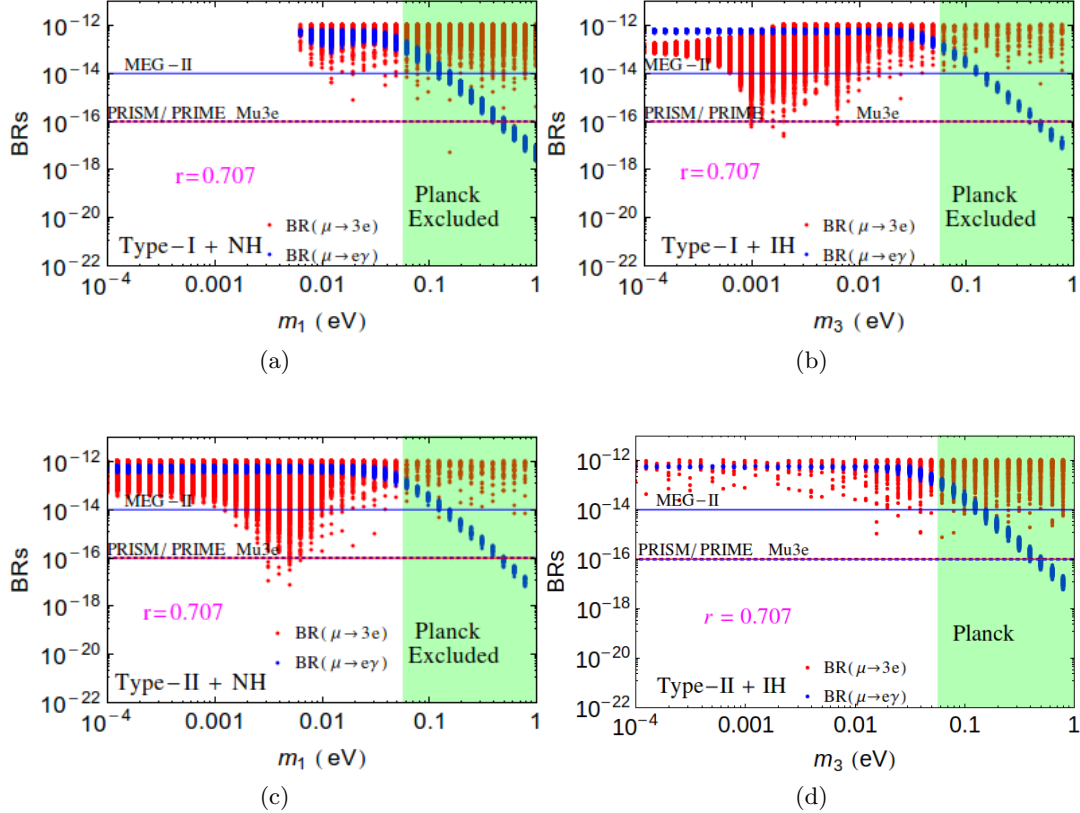


Figure 3.3: The predicted branching ratios of $\mu \rightarrow e\gamma$ (blue points) and $\mu \rightarrow 3e$ (red points) processes (when for a given light neutrino mass, current experimental bounds on the branching ratios of both are simultaneously satisfied) as a function of the lightest neutrino mass for NH (left panels) and IH (right panels) in type-I (top panels) and type-II (bottom panels) dominance. The ratio of the heaviest neutrino mass and the Higgs triplet mass has been set to $r = 0.707$. The green shaded region is disfavoured at 95% C.L. from Planck data. The blue solid horizontal line is for MEG-II sensitivity, while PRISM/PRIME and Mu3e will have sensitivities up to the blue dotted and red solid horizontal lines respectively.

ferent CP violating phases. For the line labeled as (individual absolute)², we have summed over the absolute-square of the individual contributions inside G_L^γ , G_R^γ , thereby neglecting the possibility of any interference. However, the interference terms are indeed important for the total contribution to the LFV branching ratio, as can be seen from Figure 3.4. The phase variation induces a suppression in the branching ratio due to cancellation between different contributions. We highlight this particular feature with suitable choices of the CP phases $\delta = 0$ and π in Figures 3.4a and 3.4b, from which it is evident that, while the (individual absolute)² increases with the lightest neutrino mass, the contributions G_L^γ , G_R^γ as well as the total $BR(\mu \rightarrow e\gamma)$ decrease for quasi-degenerate light neutrino masses. Similar feature is visible for $\mu \rightarrow 3e$ process, as depicted in Figures 3.4c and 3.4d. From Figures 3.4b and 3.4d, it is evident that for the Dirac CP phase $\delta = \pi$, there is an additional

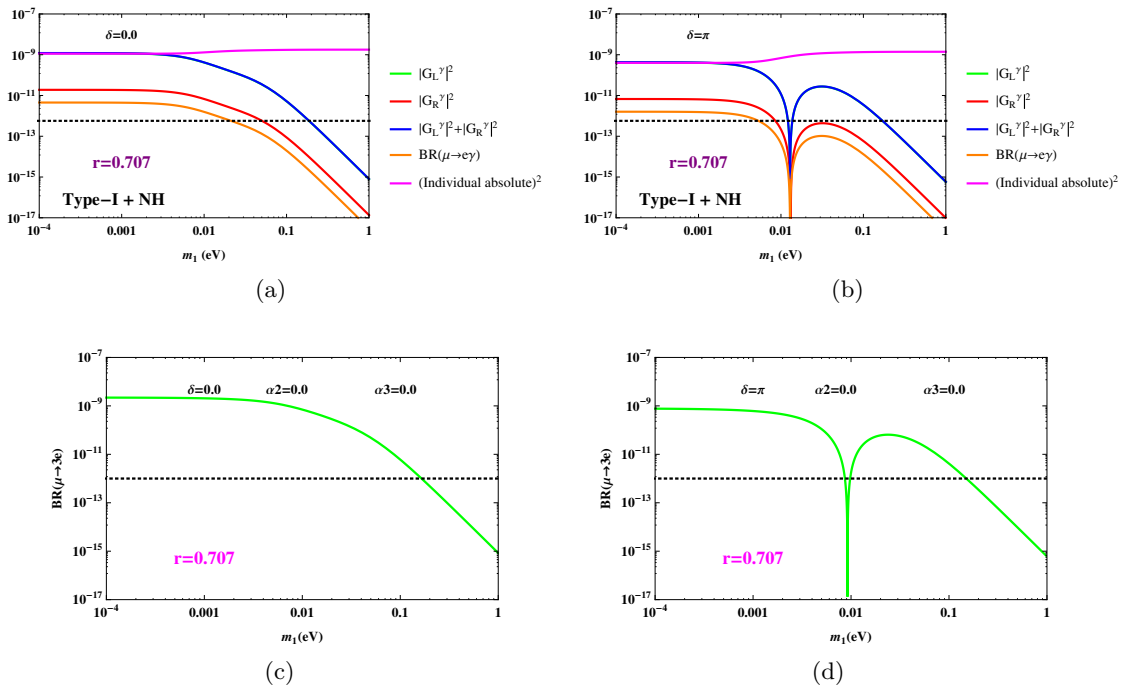


Figure 3.4: *Upper panels:* Variation of G_L^γ , G_R^γ and the total branching ratio of $\mu \rightarrow e\gamma$ process as a function of the lightest neutrino mass for $\delta = 0$ (left) and π (right). *Lower panels:* Variation of the branching ratio of $\mu \rightarrow 3e$ as a function of the lightest neutrino mass for $\delta = 0$ (left) and π (right). Here we have chosen $\alpha_2 = 0$, $\alpha_3 = 0$, $r = 0.707$, type-I dominance and NH case.

suppression in the branching ratios of $\mu \rightarrow e\gamma$ and $\mu \rightarrow 3e$ near $m_1 \sim 0.01$ eV due to an exact cancellation between different terms.

Case-II: Smaller value of r

Next we consider the case where $M_N = 500$ GeV and $M_{\text{scalar}} = 5$ TeV, leading to $r = 0.1414$. For such a heavy Higgs triplet, we expect its contribution to LFV processes to be relatively smaller, thereby allowing more LRSB parameter space for hierarchical neutrinos. This is indeed the case, as shown in Figure 3.5. A few comments are in order: (i) For the process $\mu \rightarrow e\gamma$, the predicted branching ratio is beyond the reach of MEG-II upgrade [74] excepting for type-I dominance and NH [cf. Figure 3.5a], where hierarchical m_1 ($\lesssim 0.01$ eV) may just be within its reach. However, for the process $\mu \rightarrow 3e$, the predicted branching ratios are within the experimental reach of Mu3e [76]. (ii) For the scenarios shown in Figures 3.5a–3.5c, an additional suppression occurs due to phase cancellation in the branching ratio of $\mu \rightarrow 3e$ for $m_{\text{lightest}} \sim 10^{-3} - 10^{-2}$ eV, thereby making part of the allowed parameter space beyond the reach of the Mu3e sensitivity. However, the type-II dominance IH cases is not affected by such phase-cancellation [cf. Figure 3.5d], and hence, can be tested more easily in future.

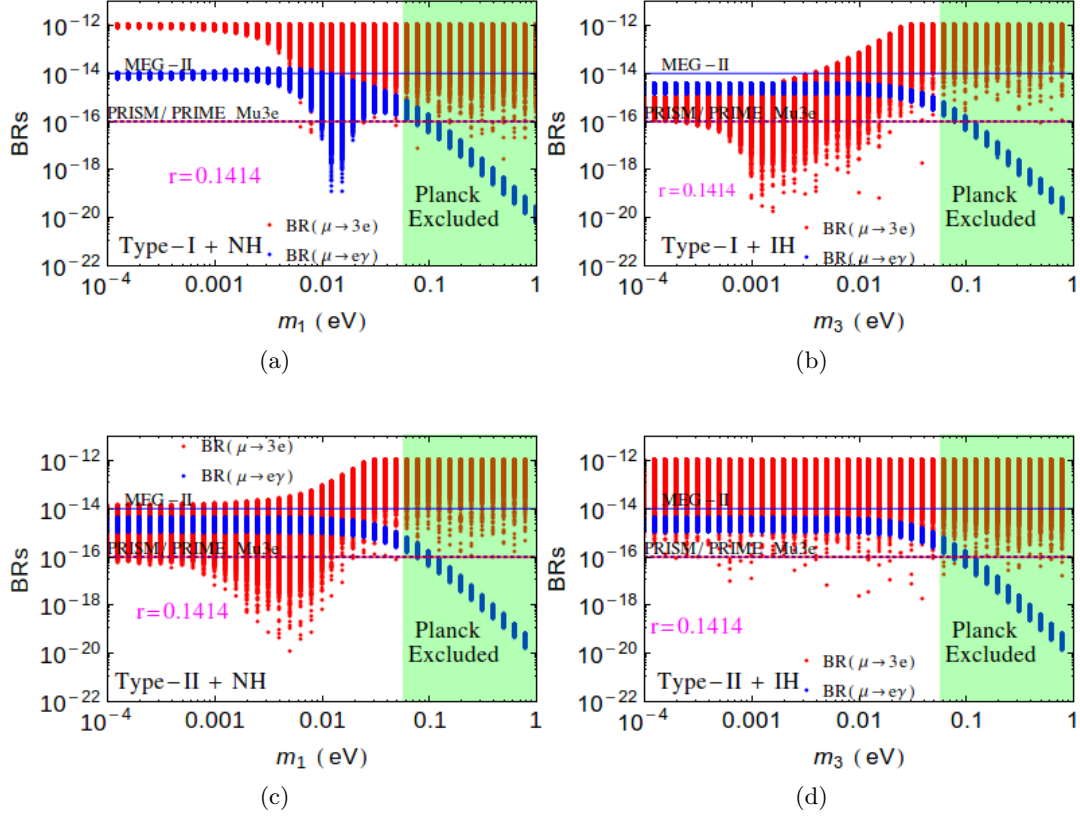


Figure 3.5: The predicted branching ratios of $\mu \rightarrow e\gamma$ (blue points) and $\mu \rightarrow 3e$ (red points) processes as a function of the lightest neutrino mass for NH (left panels) and IH (right panels) in type-I (top panels) and type-II (bottom panels) dominance. The ratio of the heaviest neutrino mass and the Higgs triplet mass has been set to $r = 0.1414$. The green shaded region is disfavoured at 95% C.L. from Planck data. The blue solid horizontal line is for MEG-II sensitivity, while PRISM/PRIME and Mu3e will have sensitivities up to the blue dotted and red solid horizontal lines respectively.

Case-III: Larger value of r

In Figure 3.6, we show the prediction for the other interesting regime, *i.e.*, lighter Higgs triplet and heavier RH neutrinos. We consider $M_N = 500$ GeV and $M_{\text{scalar}} = 500$ GeV, so that $r = 1.414$. In this case, the predicted LFV rates will be much larger than the previous two cases, due to a large triplet contribution. Hence, this scenario is heavily constrained from present experimental constraints. It is evident from Figure 3.6 that the predicted branching ratios are in agreement with the experimental LFV rates, only for quasi-degenerate mass regime, which is already disfavoured by the cosmological constraints from Planck.

Depending on the value of r , one can also obtain some constraints on the Majorana phase α_2 from the LFV bounds, as illustrated in Figure 3.7 for the type-I NH case with

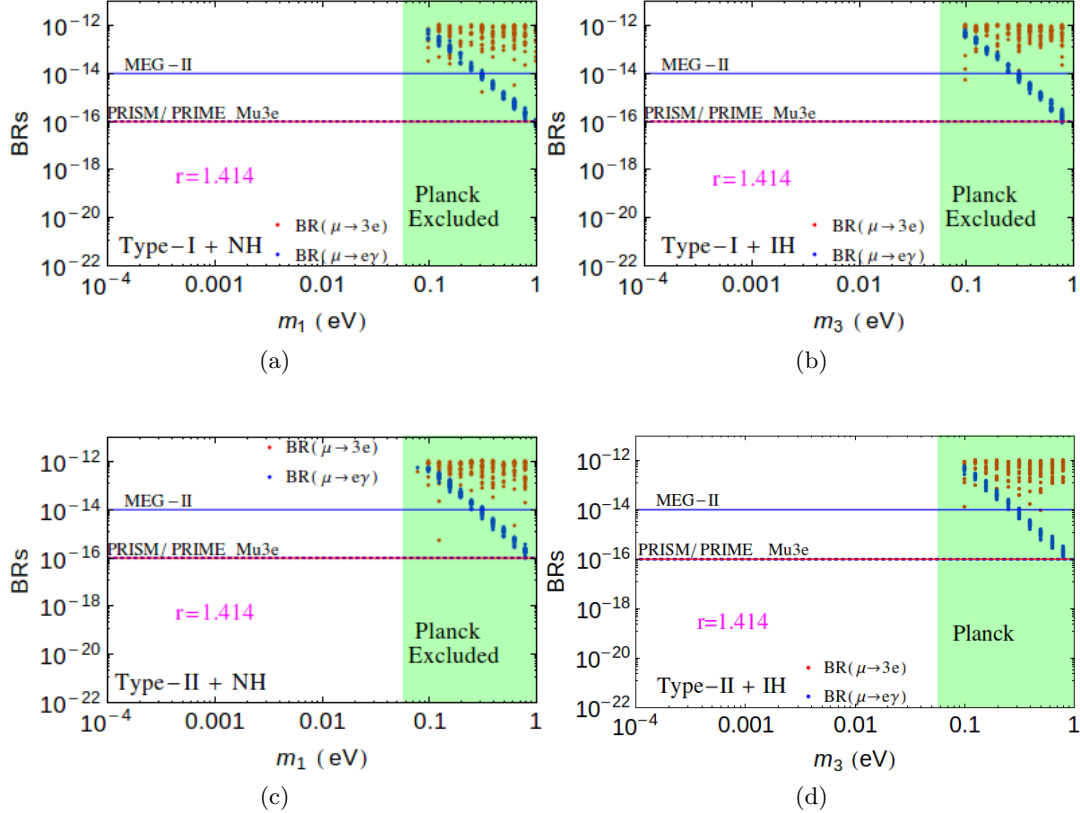


Figure 3.6: The predicted branching ratios of $\mu \rightarrow e\gamma$ (blue points) and $\mu \rightarrow 3e$ (red points) processes as a function of the lightest neutrino mass for NH (left panels) and IH (right panels) in type-I (top panels) and type-II (bottom panels) dominance. The ratio of the heaviest neutrino mass and the Higgs triplet mass has been set to $r = 1.414$. The green shaded region is disfavoured at 95% C.L. from Planck data. The blue solid horizontal line is for MEG-II sensitivity, while PRISM/PRIME and Mu3e will have sensitivities up to the blue dotted and red solid horizontal lines respectively.

$M_N = 500$ GeV. The oscillation parameters are varied as before and m_1 is varied in the range 10^{-4} eV to 1 eV. Figure 3.7a shows that for $r = 0.01414$, corresponding to $M_{\text{scalar}} = 50$ TeV, there are no constraints from LFV processes as for such a heavy mass, the triplet is effectively decoupled. As the value of r increases the allowed values of α_2 start getting restricted from LFV constraints and the preferred values for α_2 are seen to cluster around 0 and π . For $r = 1.414$, the LFV constraints are stronger and the density of the points is lesser. We did not find any such constraints on the phase α_1 from the LFV muon decays.

To summarize our findings in this section, values of r up to $\mathcal{O}(1)$ can be still allowed by the LFV constraints, depending on other parameters in the light neutrino mass matrix. This is illustrated with respect to the variation in r in Figure 3.8, where the scattered points simultaneously satisfy both $\mu \rightarrow e\gamma$ and $\mu \rightarrow 3e$ constraints for $M_N = 500$ GeV.

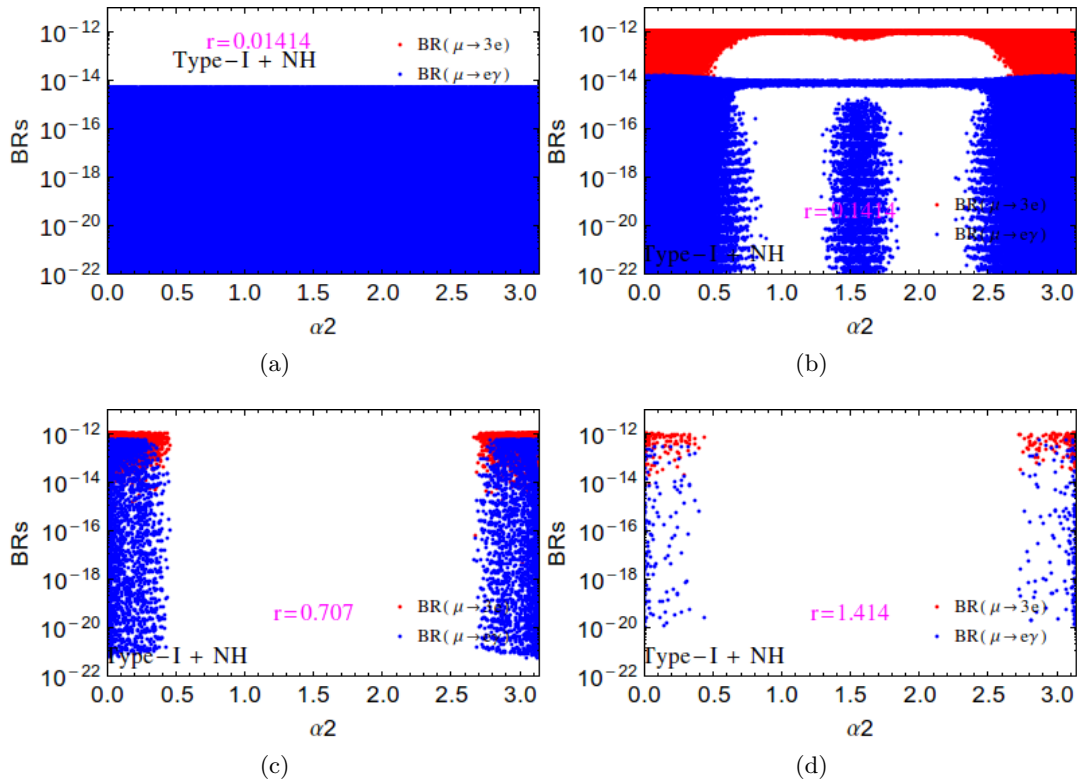


Figure 3.7: The predicted branching ratios of $\mu \rightarrow e\gamma$ (blue points) and $\mu \rightarrow 3e$ (red points) processes, when experimental bounds on the branching ratios of both are simultaneously satisfied, as a function of the Majorana phase α_2 for type-I NH case and with different values of r .

4 Neutrinoless double beta decay

In a TeV-scale LRSM, there are several new contributions to the LNV process of $0\nu\beta\beta$ [6, 30–42], due to the presence of RH currents and Higgs triplets. As discussed in the previous section, the present bounds from $\mu \rightarrow e\gamma$ and $\mu \rightarrow 3e$ still allow the heavy neutrino to Higgs triplet masses as large as $\mathcal{O}(1)$. So the Higgs triplet contribution to $0\nu\beta\beta$ can in principle be sizeable and should not be neglected. In our subsequent discussion of $0\nu\beta\beta$, we therefore take into account the Higgs triplet contribution from Δ_R . The contribution from the other Higgs triplet Δ_L is suppressed by the light neutrino mass. Also we assume the mixing between the LH and RH sectors to be small, so that their contributions to $0\nu\beta\beta$ can be neglected.

Thus, in our case, the half-life of $0\nu\beta\beta$ only includes purely LH and RH contributions:

$$\frac{1}{T_{1/2}^{0\nu}} = G_{01}^{0\nu} \left(\left| \mathcal{M}_{\nu}^{0\nu} \eta_{\nu} \right|^2 + \left| \mathcal{M}_N^{0\nu} \eta_R \right|^2 \right), \quad (4.1)$$

where $G_{01}^{0\nu}$ is the phase space factor and $\mathcal{M}_{\nu,N}^{0\nu}$ are the relevant nuclear matrix elements (NMEs) for light and heavy neutrino contributions, respectively. The particle physics pa-

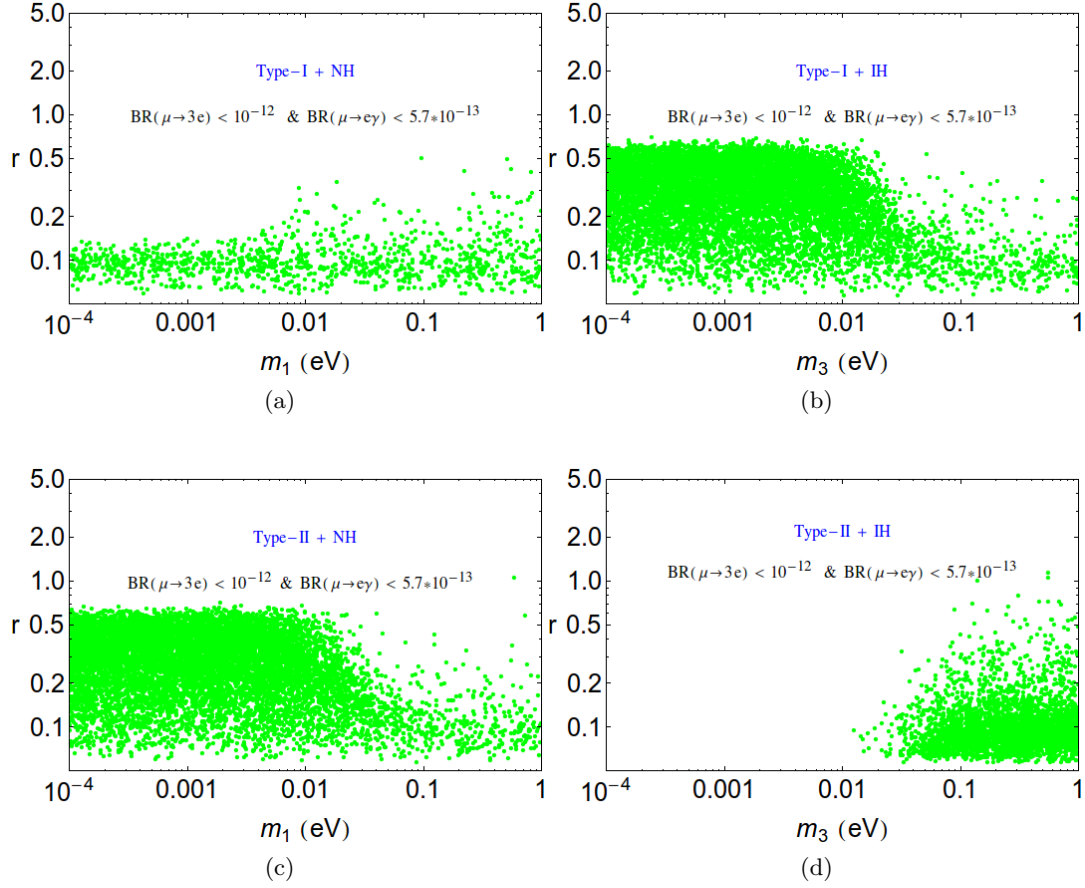


Figure 3.8: The allowed parameter space as a function of r satisfying both $\mu \rightarrow e\gamma$ and $\mu \rightarrow 3e$ constraints simultaneously.

parameters η_ν and η_R correspond to the LH and RH amplitudes, respectively (*cf.* Figure 4.1):

$$\eta_\nu = \frac{1}{m_e} \sum_{i=1}^3 U_{ei}^2 m_i, \quad \eta_R = m_p \left(\frac{m_{W_L}}{m_{W_R}} \right)^4 \left(\sum_{i=1}^3 \frac{V_{ei}^2}{M_i} + \sum_{i=1}^3 \frac{V_{ei}^2 M_i}{m_{\Delta_R^{++}}^2} \right), \quad (4.2)$$

where m_e and m_p are the masses of electron and proton, respectively. The corresponding effective neutrino mass is given by

$$m_{ee} = \sum_i U_{ei}^2 m_i + \langle p^2 \rangle \left(\frac{m_{W_L}}{m_{W_R}} \right)^4 \left(\sum_i \frac{V_{ei}^2}{M_i} + \sum_i \frac{V_{ei}^2 M_i}{m_{\Delta_R^{++}}^2} \right), \quad (4.3)$$

where $\langle p^2 \rangle = m_e m_p \mathcal{M}_N^{0\nu} / \mathcal{M}_\nu^{0\nu} \sim (153 - 184 \text{ MeV})^2$ for ^{76}Ge isotope [83] which we have taken as our reference nucleus in this analysis.

In Figure 4.2, we show the effective mass m_{ee} versus the lightest neutrino mass m_1 for type-I dominance with NH and for different values of the ratio r . In this and all other figures in this section for obtaining the effective mass, we have used only those values of the

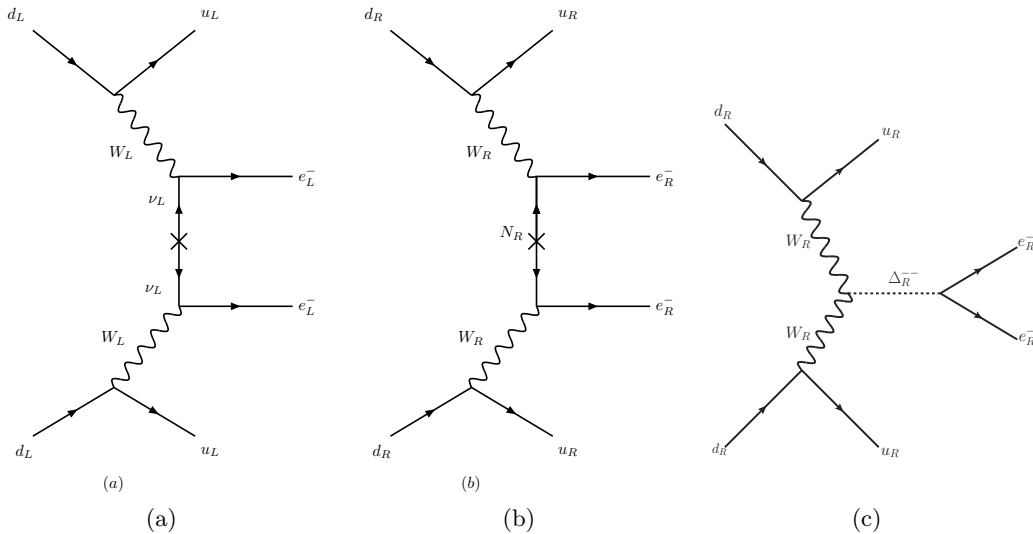


Figure 4.1: The dominant LH and RH current contributions to the $0\nu\beta\beta$ process in the LRSM with small LH-RH mixing.

model parameters that are consistent with the experimental limits of $\mu \rightarrow e\gamma$ and $\mu \rightarrow 3e$ processes, as discussed in Section 3. Thus these plots are inclusive of the LFV constraints. We have included the 3σ variation of the oscillation parameters from Ref. [81], as well as the NME uncertainties as reported in Ref. [83].

Figure 4.2a is for $r = 0.01414$ ($M_N = 500$ GeV, $M_{\text{scalar}} = 50$ TeV). Such a heavy triplet is almost decoupled, and hence, there are no additional constraints on $0\nu\beta\beta$ from the LFV processes. Thus in this case, the effective mass m_{ee} is the same as that obtained in Refs. [34, 39] without including the triplet contribution. Note however that, although there are no constraints from LFV processes, the current $0\nu\beta\beta$ bounds from GERDA [84] disfavour lower (fully hierarchical) and higher (quasi-degenerate) values of m_1 . The quasi-degenerate region is also disfavoured from Planck data. The future limits from GERDA-II [85] could even place a stronger *lower* limit on the lightest neutrino mass in this scenario.

As we go to a higher value of $r = 0.1414$ ($M_N = 500$ GeV, $M_{\text{scalar}} = 5$ TeV), as shown in Figure 4.2b, the current LFV constraints (see Figure 3.5) still allow the whole range of m_1 . However, there are additional constraints on the Majorana phase α_2 as has been shown in Figure 3.7. This rules out a part of the parameter space involving the cancellation region, and therefore, very low values of m_{ee} can no longer be obtained. The shape of the curve for $|m_{ee}|$ in Figure 4.2b can be solely attributed to the LFV constraints on the Majorana phases. We have checked that if LFV constraints are not included, then Figure 4.2b replicates Figure 4.2a.

For smaller Higgs triplet masses that lead to larger value of r , such as, $r = 0.707$ and 1.1414 , the hierarchical mass range $m_1 \leq 0.01$ eV is completely ruled out and only the quasi-degenerate region is allowed by the LFV constraints, as shown in the first panel corresponding to type-I NH in Figure 3.3 and Figure 3.6. The corresponding impact of the LFV constraints on the prediction for $0\nu\beta\beta$ is clearly visible from Figure 4.2c and

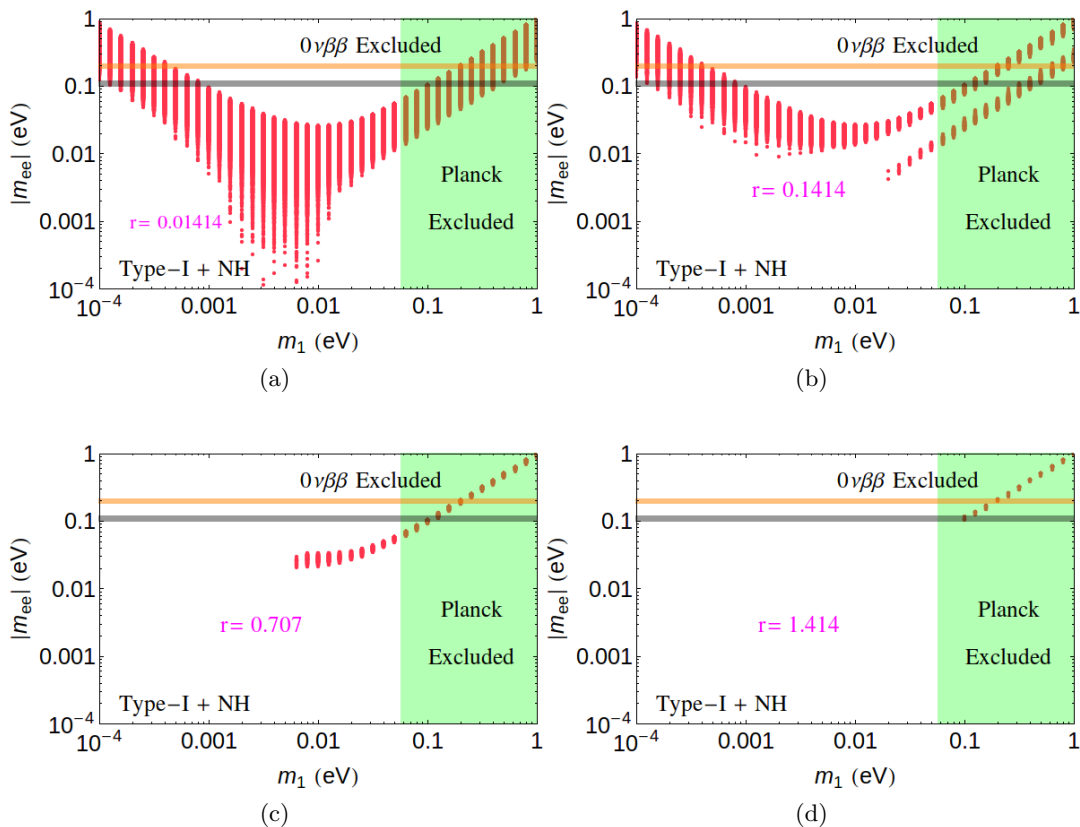


Figure 4.2: The variation of the effective neutrino mass as a function of the lightest neutrino mass for type-I dominance with NH. The different panels correspond to different values of r . The green shaded area is disfavoured at 95% C.L. by Planck. The orange band corresponds to the range of $|m_{ee}| = 0.18 - 0.22$ eV, the region above which is excluded at 90% C.L. by the combined limit from GERDA. The black band corresponds to the future limit ($|m_{ee}| = 0.098 - 0.12$ eV) from GERDA-II.

Figure 4.2d, where the effective mass is in agreement with the LFV constraints mostly for quasi-degenerate light neutrino masses. Note that most of this region is already disfavoured by the Planck data and/or the current upper limit on m_{ee} from GERDA. For $r=0.707$ a small window for m_1 ($\sim 0.005 - 0.05$ eV) still exists which is consistent with all the current constraints. However this region is beyond the reach of GERDA-II and might be accessible only with future ton-scale experiments, such as MAJORANA+GERDA [86].

Similarly, in Figures 4.3, 4.4 and 4.5, we show the effective mass versus lightest neutrino mass for the case of type-I dominance with IH, type-II dominance with NH and IH, respectively. In all these scenarios, the $r = 0.01414$ case again resembles to the cases where the Higgs triplet effect is not included [34, 39]. Also note that for these plots the cancellation region with very low value of m_{ee} is not obtained. The exclusion of certain regions of parameter space specially for higher values of the lightest neutrino mass is due to the constraint on the phase α_2 from LFV processes, as explicitly shown in Figure 3.7.

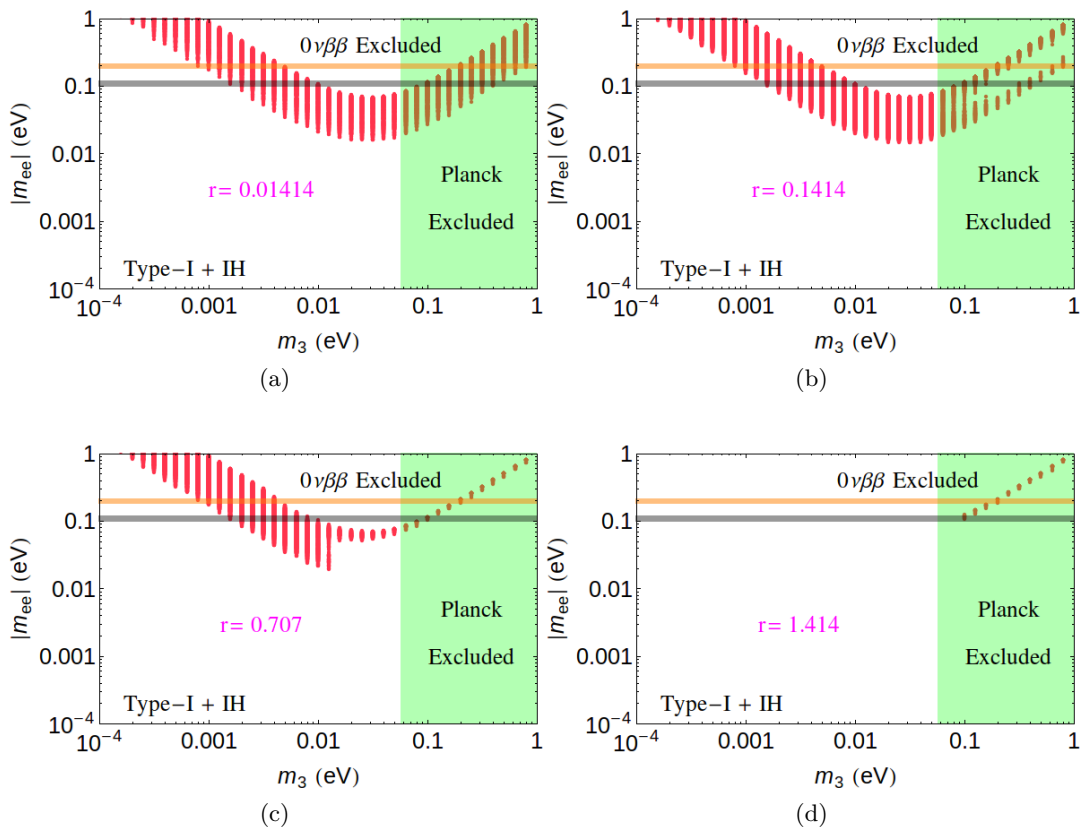


Figure 4.3: The variation of the effective mass as a function of the lightest neutrino mass for type-I dominance and IH. The different panels correspond to different values of r . The green shaded area is disfavoured at 95% C.L. by Planck. The orange band corresponds to the range of $|m_{ee}| = 0.18 - 0.22$ eV, the region above which is excluded at 90% C.L. by the combined limit from GERDA. The black band corresponds to the future limit ($|m_{ee}| = 0.098 - 0.12$ eV) from GERDA-II. The bands are due to the NME uncertainties.

From Figures 4.2, 4.3, 4.4 and 4.5, it is evident that a large value of r is highly constrained experimentally, whereas a moderate value of $r \lesssim \mathcal{O}(1)$ is more favourable and can be tested in the next generation $0\nu\beta\beta$ experiments, such as GERDA-II [85], in combination with the future LFV experiments.

Finally in Figure 4.6, we show the allowed region in the M_N versus M_{scalar} plane that is experimentally allowed by both LFV and $0\nu\beta\beta$ constraints. Here we have set $g_L = g_R$ and $m_{W_R} = 3.5$ TeV to satisfy the direct search constraints from the LHC [51, 52]. The blue shaded regions correspond to the case with $M_N, M_{\text{scalar}} \leq m_{W_R}$, which are favoured by vacuum stability and perturbative arguments [87, 88]. The green points are after satisfying the LFV constraints, while the red points also satisfy the current upper bound on effective mass $m_{ee} < 0.18$ eV. It is evident that M_N and M_{scalar} values below 500 GeV or so are disfavoured by the low-energy constraints, whereas heavier triplet masses are still allowed, as long as the corresponding Yukawa couplings are below the perturbative limit.

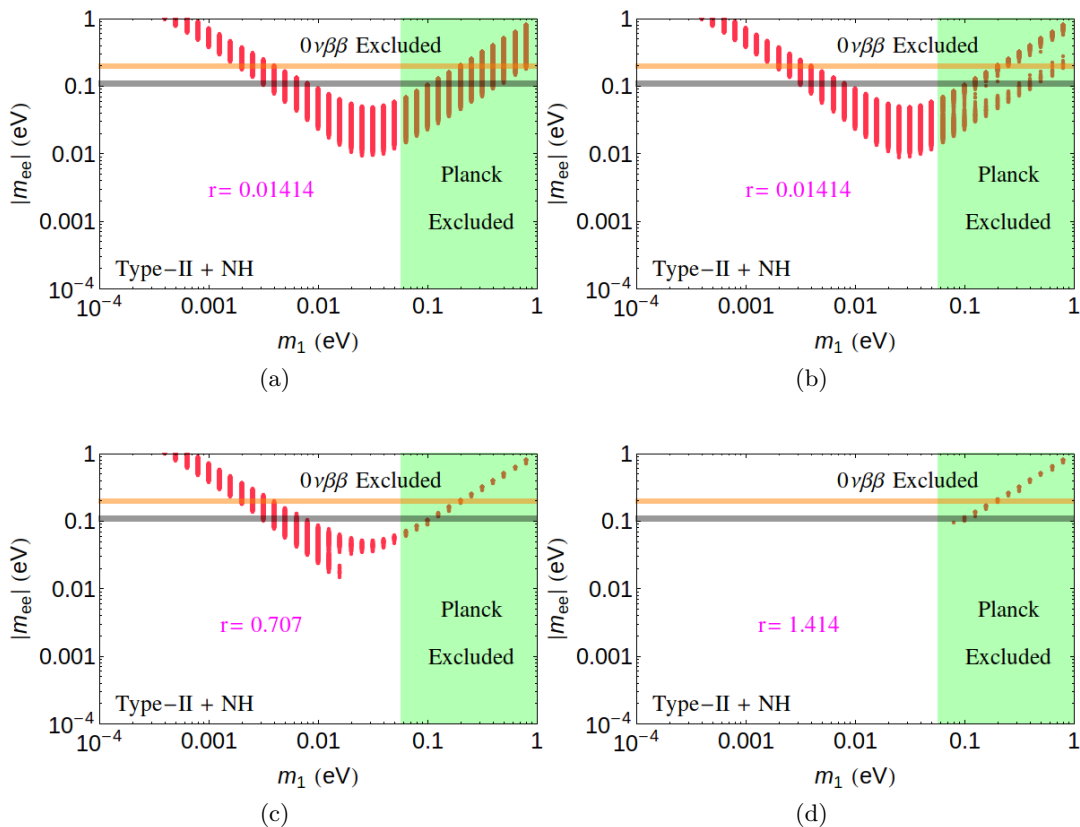


Figure 4.4: The variation of the effective mass as a function of the light neutrino mass for type-II dominance and NH. The orange band corresponds to the range of $|m_{ee}| = 0.18\text{--}0.22$ eV, the region above which is excluded at 90% C.L. by the combined limit from GERDA. The black band corresponds to the future limit ($|m_{ee}| = 0.098\text{--}0.12$ eV) from GERDA-II.

5 Diboson excess

A number of recent resonance searches with the $\sqrt{s} = 8$ TeV LHC data have observed excess events around an invariant mass of 2 TeV, the most notable one being a 3.4σ local excess in the ATLAS search [89, 90] for a heavy resonance decaying into a pair of SM gauge bosons, followed by the hadronic decay of the diboson system.³ It is known that this diboson excess can be *naturally* explained by a TeV-scale LRSM for the RH gauge boson mass $m_{W_R} \sim 2$ TeV and the corresponding gauge coupling $g_R \sim 0.4\text{--}0.5$ [93–100].

In this section, we study the implications of the diboson excess on the predictions of LFV and $0\nu\beta\beta$. A similar study was performed in Ref. [42], but here we also include the triplet contribution. For the gauge couplings $g_R \neq g_L$, the branching ratio of the LFV process $\mu \rightarrow e\gamma$ is given by Eq. (3.1), where the factors G_L^γ and G_R^γ are scaled by a factor

³Although no such excess above 2σ has been found in the early $\sqrt{s} = 13$ TeV data, the sensitivity is too small to rule out the Run I excess at the 95% CL [91, 92] and we have to wait for more data from the Run-II phase to confirm/discard this excess.

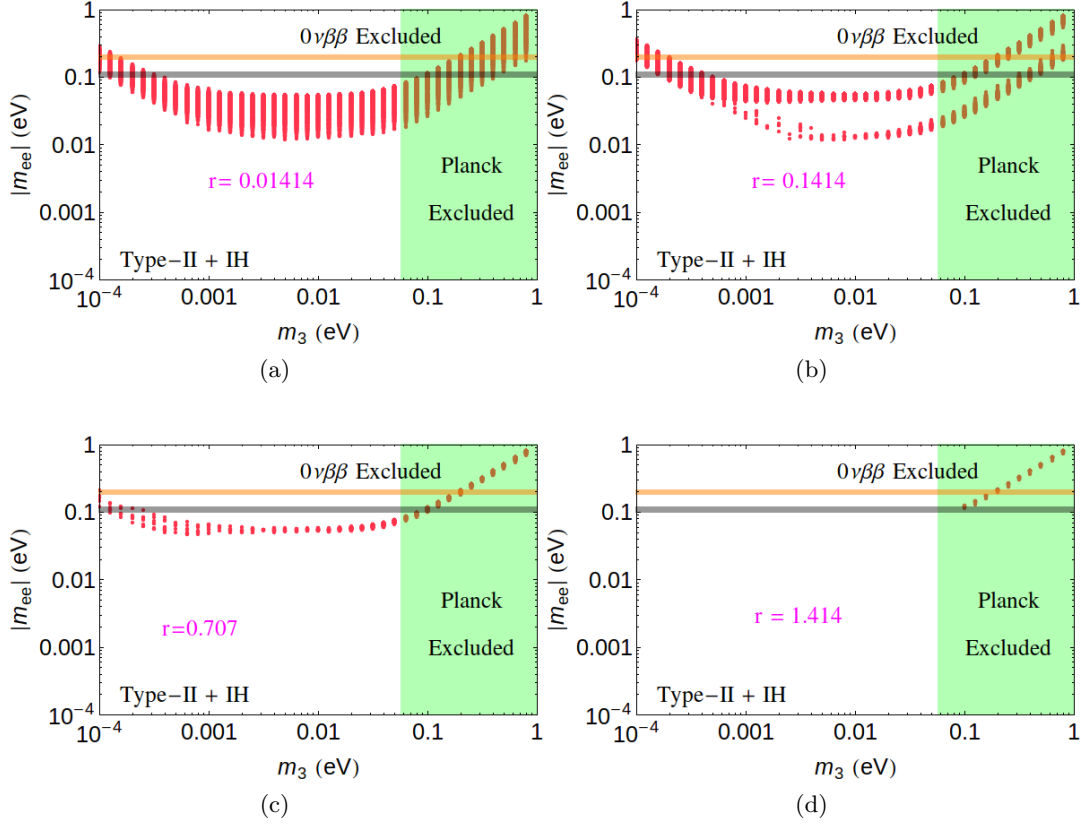


Figure 4.5: The variation of the effective mass as a function of the lightest neutrino mass for type-II dominance and IH. The different panels correspond to different values of r . The green shaded area is disfavoured at 95% C.L. by Planck. The orange band corresponds to the range of $|m_{ee}| = 0.18 - 0.22$ eV, the region above which is excluded at 90% C.L. by the combined limit from GERDA. The black band corresponds to the future limit ($|m_{ee}| = 0.098 - 0.12$ eV) from GERDA-II.

of with respect to those given in Eqs. (3.2) and (3.3), *i.e.*,

$$G_R^\gamma \simeq \left(\frac{g_R}{g_L}\right)^2 \sum_i V_{\mu i} V_{ei}^* \left(\frac{m_{WL}^2}{m_{WR}^2} G_1^\gamma(b_i) + \frac{2b_i}{3} \frac{m_{WL}^2}{m_{\Delta_R^{++}}^2} \right), \quad (5.1)$$

$$G_L^\gamma \simeq \left(\frac{g_R}{g_L}\right)^2 \sum_i V_{\mu i} V_{ei}^* b_i \left(\frac{2}{3} \frac{m_{WL}^2}{m_{\Delta_L^{++}}^2} G_1^\gamma(b_i) + \frac{1}{12} \frac{m_{WL}^2}{m_{\Delta_L^+}^2} \right). \quad (5.2)$$

Similarly, the effective mass for $0\nu\beta\beta$ [*c.f.*, Eq. (4.3)] will be of the following form:

$$m_{ee} = \sum_i U_{ei}^2 m_i + \left(\frac{g_R}{g_L}\right)^4 \langle p^2 \rangle \left(\frac{m_{WL}}{m_{WR}}\right)^4 \left(\sum_i \frac{V_{ei}^2}{M_i} + \sum_i \frac{V_{ei}^2 M_i}{m_{\Delta_R^{++}}^2} \right). \quad (5.3)$$

In Figures 5.1 and 5.2, we show the branching ratios of $\mu \rightarrow e\gamma$, $\mu \rightarrow 3e$ processes and the effective mass m_{ee} for the RH gauge boson mass $m_{WR} = 2$ TeV. Comparing Figure 5.1

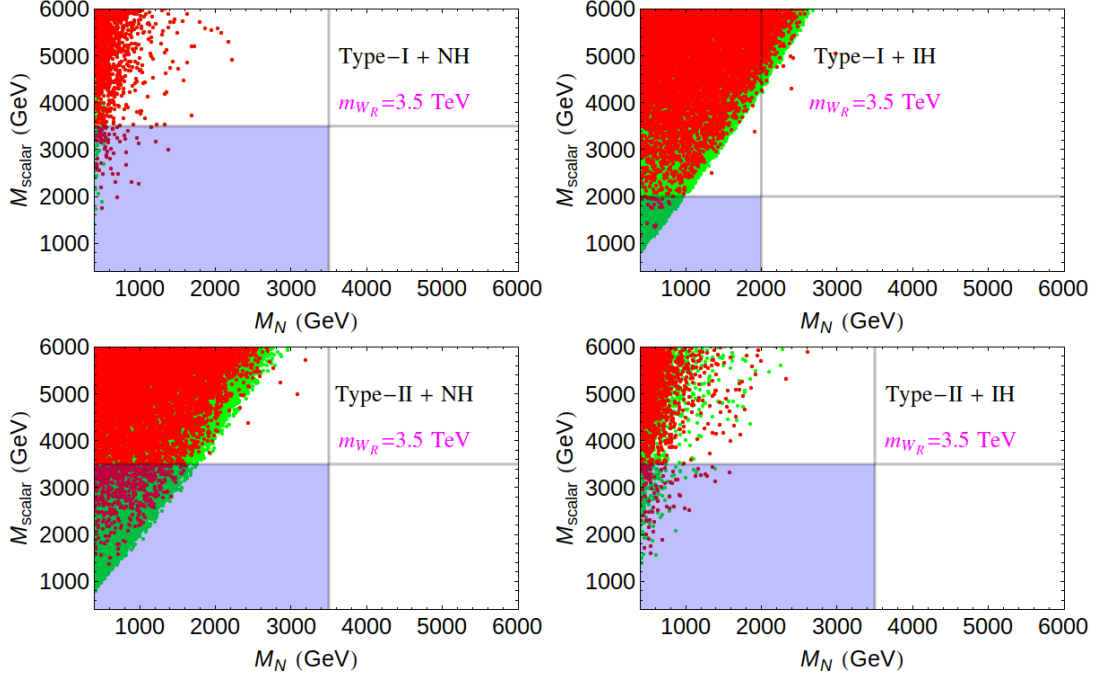


Figure 4.6: The allowed region in the M_N vs M_Δ plane that is experimentally allowed by LFV processes, as well as $0\nu\beta\beta$, for $m_{W_R} = 3.5$ TeV. The green points are after satisfying the LFV constraints, while the red points also satisfy the current upper bound on effective mass $m_{ee} < 0.18$ eV. The blue shaded regions correspond to the natural case with $M_N, M_{\text{scalar}} \leq m_{W_R}$.

with Figure 3.3 (for $m_{W_R} = 3.5$ TeV), it is evident that even a moderate value of $r = 0.707$ is now severely constrained. This is also reflected in Figure 5.2 from $0\nu\beta\beta$ limits.

Finally in Figure 5.3, we show the allowed region in the M_N versus M_{scalar} plane that is experimentally allowed by LFV processes, as well as by $0\nu\beta\beta$, while explaining the diboson excess. As in Figure 4.6, the blue shaded regions correspond to the natural case with $M_N, M_{\text{scalar}} \leq m_{W_R}$ [87, 88]. The green points are after satisfying the LFV constraints, while the red points also satisfy the current upper bound on effective mass $m_{ee} < 0.18$ eV.

6 Summary

We have studied the correlated constraints from low-energy LFV and $0\nu\beta\beta$ processes for a TeV scale LRSM including the contribution of the Higgs triplets. Triplet masses comparable to or lighter than the RH neutrino masses were previously thought to be completely ruled out by the LFV constraints. We show that even with relatively lower values of triplet masses, it is still possible to get allowed parameter regions consistent with the LFV limits due to the existence of cancellations between different contributions predominantly in the quasi-degenerate region which can be attributed to the so far unknown CP phases. We illustrate this effect in a simplified scenario of the LRSM in type-I and type-II seesaw dominance limits for both normal and inverted mass hierarchies, by fixing the RH gauge

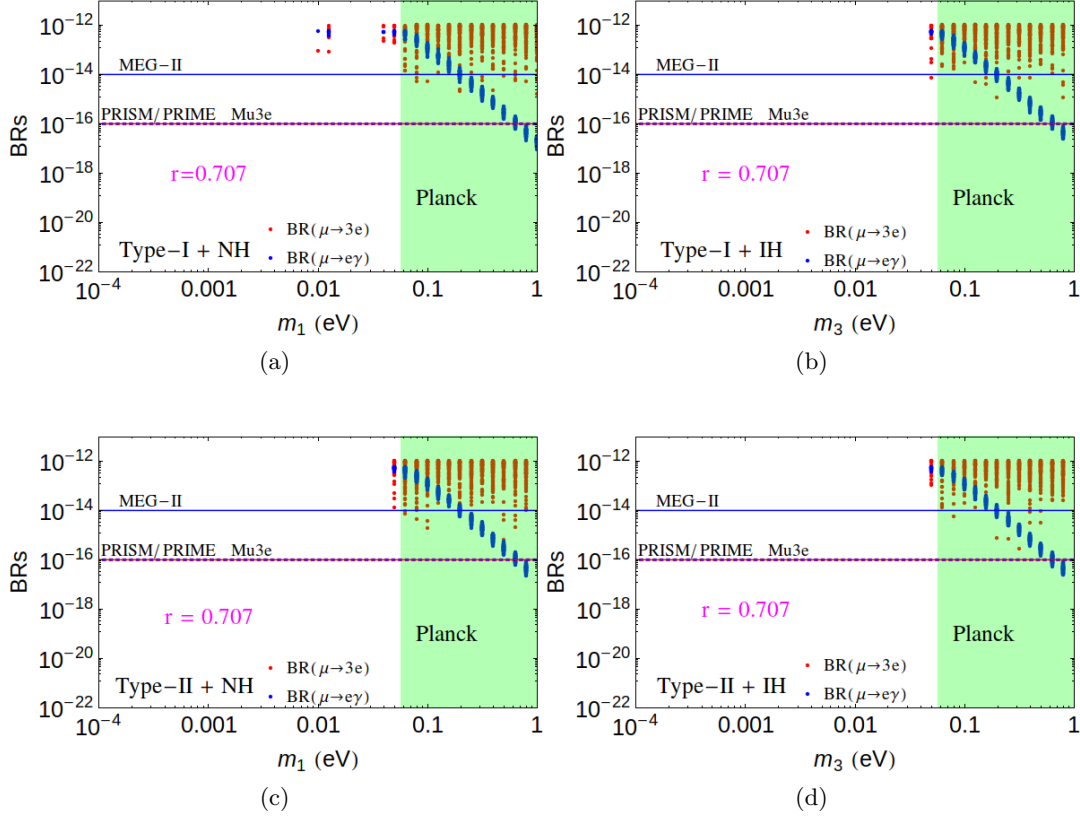


Figure 5.1: The branching ratio of $\mu \rightarrow e\gamma$ and $\mu \rightarrow 3e$ vs light neutrino mass, for the right-handed gauge boson mass $m_{W_R} = 2$ TeV and $r = 0.707$.

boson mass $m_{W_R} = 3.5$ TeV and the heaviest RH neutrino mass $M_N = 500$ GeV, and varying the triplet mass M_Δ in terms of the ratio $r = M_N/M_\Delta$. We find that for small values of $r \lesssim 0.1$, the triplet contributions to the LFV observables are negligible (see Figure 3.5), in agreement with the previous studies. However, for moderate values of $0.1 \lesssim r \lesssim 1$, the triplet contribution rules out only a part of the LRSM parameter space. In particular, a hierarchical light neutrino spectrum with $m_1 \lesssim 0.01$ eV is disfavoured from LFV constraints for type-I NH scenario, while the type-I IH and type-II cases remain largely unconstrained, but can be accessible at future LFV experiments (see Figure 3.3). Constraints are also obtained on the Majorana phase α_2 , restricting it close to either 0 or π for most of the cases analysed here (see Figure 3.7). For larger values of $r \gtrsim 1$, LFV constraints become more stringent, ruling out the hierarchical light neutrino spectrum and only allowing the quasi-degenerate region (see Figure 3.6). However, this quasi-degenerate region is already disfavoured by the cosmological limit on the sum of light neutrino masses from Planck data, as well as from current experimental constraints on the half-life of $0\nu\beta\beta$ process. Thus, we conclude that light triplets are completely disfavoured only for $r \gtrsim 1$ (see Figure 3.8).

We also give the predictions for the effective neutrino mass for $0\nu\beta\beta$ for all the cases,

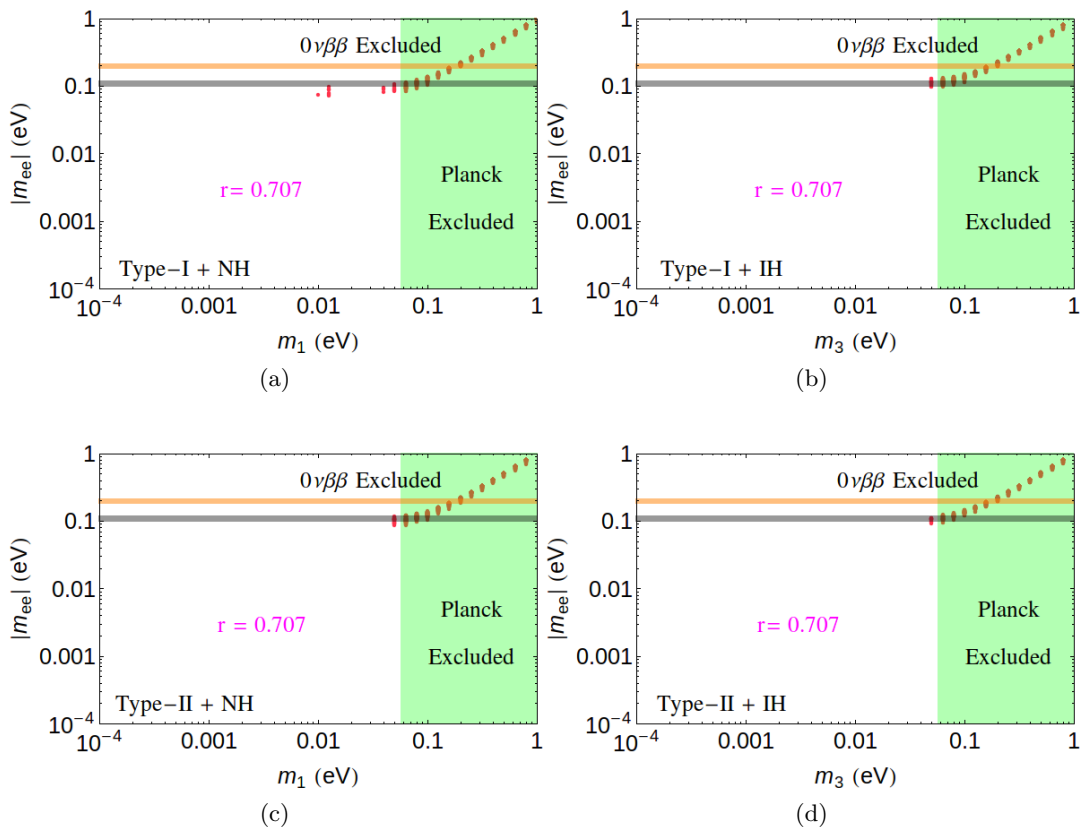


Figure 5.2: The effective mass m_{ee} vs light neutrino mass, for the right-handed gauge boson mass $m_{W_R} = 2$ TeV and $r = 0.707$. The different panels correspond to: (a) type-I dominant NH (b) type-I dominant IH (c) type-II dominant NH (d) type-II dominant IH. The orange band corresponds to the range of $|m_{ee}| = 0.18 - 0.22$ eV, the region above which is excluded at 90% C.L. by the combined limit from GERDA. The black band corresponds to the future limit ($|m_{ee}| = 0.098 - 0.12$ eV) from GERDA-II.

taking into account the LFV constraints. Again, we find that for a higher value of $r \gtrsim 1$, the LRSM parameter space is severely restricted due to the LFV constraints, while the $0\nu\beta\beta$ predictions for moderate values of $0.1 \lesssim r \lesssim 1$ are within reach of future experiments (see Figures 4.2-4.5). We emphasise that the LFV constraints on the Majorana phases play a non-trivial role in ruling out parts of the parameter space otherwise allowed by the $0\nu\beta\beta$ constraints.

Finally, we also study the triplet contribution to LFV and $0\nu\beta\beta$ for the LRSM scenario with $m_{W_R} = 2$ TeV and $g_R = 0.5$, being motivated by the recent indication of a diboson excess by the ATLAS experiment. We find that this case is more severely constrained than the $m_{W_R} = 3.5$ TeV case discussed above. However, one can find smaller values of r (see Figure 5.3) which are still consistent with the LFV and $0\nu\beta\beta$ constraints, while simultaneously explaining the ATLAS diboson anomaly. With more data pouring in from the Run-II phase of the LHC, the light triplet scenario could be probed at the energy

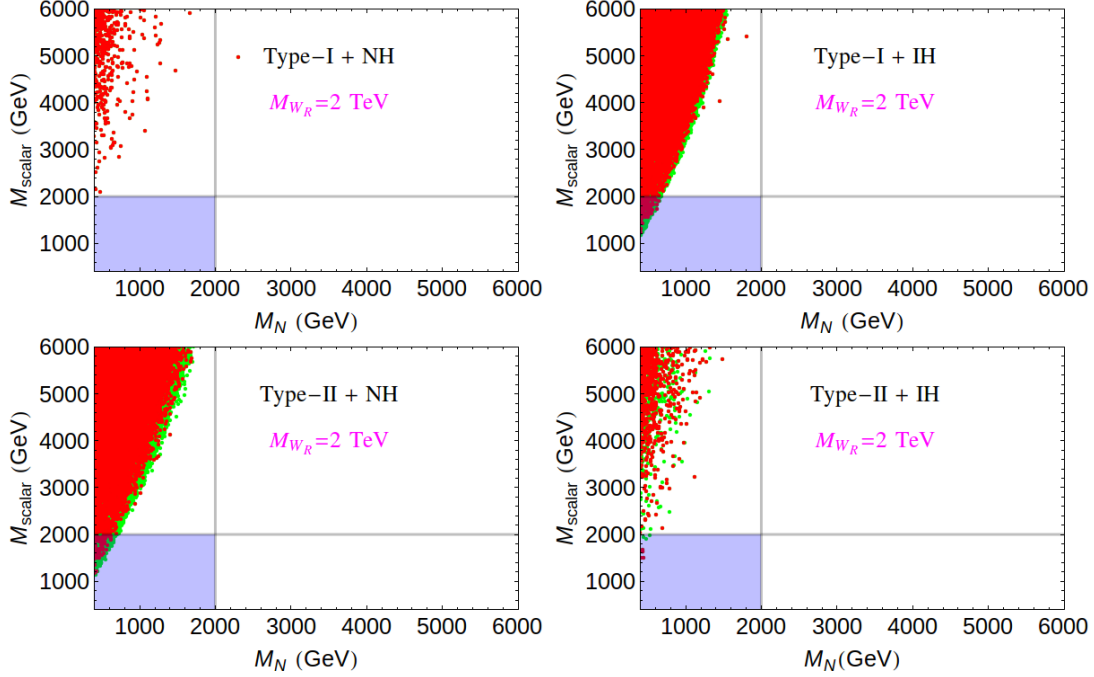


Figure 5.3: The allowed region in the M_N vs M_{scalar} plane that is experimentally allowed by LFV processes, as well as $0\nu\beta\beta$, for $m_{W_R} = 2$ TeV. The green points are after satisfying the LFV constraints, while the red points also satisfy the current upper bound on effective mass $m_{ee} < 0.18$ eV. The blue shaded regions correspond to the natural case with $M_N, M_{\text{scalar}} \leq m_{W_R}$.

frontier in near future, in conjunction with the complementary probes in future low-energy experiments at the intensity frontier.

Acknowledgments

B.D. would like to thank Werner Rodejohann for helpful discussions. This work of B.D. was supported in part by a TUM University Foundation Fellowship and the DFG cluster of excellence ‘‘Origin and Structure of the Universe’’, as well as by the DFG with grant RO 2516/5-1 during the final stages. B.D. also acknowledges the local hospitality and partial support from DESY, Hamburg where part of this work was done. M.M. would like to acknowledge the generous support provided by IISER Mohali and the DST-INSPIRE Faculty Scheme.

References

- [1] **Particle Data Group** Collaboration, K. Olive et al., *Review of Particle Physics*, *Chin.Phys.* **C38** (2014) 090001.
- [2] **ATLAS** Collaboration, G. Aad et al., *Observation of a new particle in the search for the Standard Model Higgs boson with the ATLAS detector at the LHC*, *Phys. Lett.* **B716** (2012) 1–29, [[arXiv:1207.7214](https://arxiv.org/abs/1207.7214)].

- [3] CMS Collaboration, S. Chatrchyan et al., *Observation of a new boson at a mass of 125 GeV with the CMS experiment at the LHC*, *Phys. Lett.* **B716** (2012) 30–61, [[arXiv:1207.7235](#)].
- [4] S. Weinberg, *Baryon and Lepton Nonconserving Processes*, *Phys.Rev.Lett.* **43** (1979) 1566–1570.
- [5] P. Minkowski, *$\mu \rightarrow e$ gamma at a Rate of One Out of 1-Billion Muon Decays?*, *Phys.Lett.* **B67** (1977) 421.
- [6] R. N. Mohapatra and G. Senjanovic, *Neutrino Mass and Spontaneous Parity Violation*, *Phys.Rev.Lett.* **44** (1980) 912.
- [7] T. Yanagida, *Horizontal Symmetry and Masses of Neutrinos*, *Conf.Proc.* **C7902131** (1979) 95–99.
- [8] M. Gell-Mann, P. Ramond, and R. Slansky, *Complex Spinors and Unified Theories*, *Conf.Proc.* **C790927** (1979) 315–321.
- [9] S. L. Glashow, *The Future of Elementary Particle Physics*, *NATO Sci. Ser. B* **61** (1980) 687.
- [10] M. Magg and C. Wetterich, *Neutrino Mass Problem and Gauge Hierarchy*, *Phys.Lett.* **B94** (1980) 61.
- [11] J. Schechter and J. Valle, *Neutrino Masses in $SU(2) \times U(1)$ Theories*, *Phys.Rev.* **D22** (1980) 2227.
- [12] R. N. Mohapatra and G. Senjanovic, *Neutrino Masses and Mixings in Gauge Models with Spontaneous Parity Violation*, *Phys.Rev.* **D23** (1981) 165.
- [13] G. Lazarides, Q. Shafi, and C. Wetterich, *Proton Lifetime and Fermion Masses in an $SO(10)$ Model*, *Nucl.Phys.* **B181** (1981) 287.
- [14] R. Foot, H. Lew, X. He, and G. C. Joshi, *Seesaw Neutrino Masses induced by a Triplet of Leptons*, *Z.Phys.* **C44** (1989) 441.
- [15] J. C. Pati and A. Salam, *Lepton number as the fourth "color"*, *Phys. Rev. D* **10** (1974) 275–289.
- [16] R. Mohapatra and J. C. Pati, *A Natural Left-Right Symmetry*, *Phys.Rev.* **D11** (1975) 2558.
- [17] R. N. Mohapatra and J. C. Pati, *Left-Right Gauge Symmetry and an Isoconjugate Model of CP Violation*, *Phys. Rev.* **D11** (1975) 566–571.
- [18] G. Senjanovic and R. N. Mohapatra, *Exact Left-Right Symmetry and Spontaneous Violation of Parity*, *Phys.Rev.* **D12** (1975) 1502.
- [19] W.-Y. Keung and G. Senjanovic, *Majorana Neutrinos and the Production of the Right-handed Charged Gauge Boson*, *Phys.Rev.Lett.* **50** (1983) 1427.
- [20] A. Ferrari et al., *Sensitivity study for new gauge bosons and right-handed Majorana neutrinos in pp collisions at $\sqrt{s} = 14$ -TeV*, *Phys.Rev.* **D62** (2000) 013001.
- [21] M. Nemevsek, F. Nesti, G. Senjanovic, and Y. Zhang, *First Limits on Left-Right Symmetry Scale from LHC Data*, *Phys.Rev.* **D83** (2011) 115014, [[arXiv:1103.1627](#)].
- [22] J. Chakraborty, J. Gluza, R. Sevvillano, and R. Szafron, *Left-Right Symmetry at LHC and Precise 1-Loop Low Energy Data*, *JHEP* **1207** (2012) 038, [[arXiv:1204.0736](#)].

- [23] S. Das, F. Deppisch, O. Kittel, and J. Valle, *Heavy Neutrinos and Lepton Flavour Violation in Left-Right Symmetric Models at the LHC*, *Phys.Rev.* **D86** (2012) 055006, [[arXiv:1206.0256](#)].
- [24] J. A. Aguilar-Saavedra and F. R. Joaquim, *Measuring heavy neutrino couplings at the LHC*, *Phys. Rev.* **D86** (2012) 073005, [[arXiv:1207.4193](#)].
- [25] C.-Y. Chen, P. S. B. Dev, and R. N. Mohapatra, *Probing Heavy-Light Neutrino Mixing in Left-Right Seesaw Models at the LHC*, *Phys. Rev.* **D88** (2013) 033014, [[arXiv:1306.2342](#)].
- [26] J. Gluza and T. Jeliński, *Heavy neutrinos and the $pp \rightarrow lljj$ CMS data*, *Phys. Lett.* **B748** (2015) 125–131, [[arXiv:1504.05568](#)].
- [27] P. S. B. Dev, D. Kim, and R. N. Mohapatra, *Disambiguating Seesaw Models using Invariant Mass Variables at Hadron Colliders*, [arXiv:1510.04328](#).
- [28] G. Senjanovic, *Seesaw at LHC through Left - Right Symmetry*, *Int. J. Mod. Phys.* **A26** (2011) 1469–1491, [[arXiv:1012.4104](#)].
- [29] F. F. Deppisch, P. S. B. Dev, and A. Pilaftsis, *Neutrinos and Collider Physics*, *New J. Phys.* **17** (2015), no. 7 075019, [[arXiv:1502.06541](#)].
- [30] R. N. Mohapatra and J. D. Vergados, *A New Contribution to Neutrinoless Double Beta Decay in Gauge Models*, *Phys. Rev. Lett.* **47** (1981) 1713–1716.
- [31] C. E. Picciotto and M. S. Zahir, *Neutrinoless Double Beta Decay in Left-right Symmetric Models*, *Phys. Rev.* **D26** (1982) 2320.
- [32] M. Hirsch, H. V. Klapdor-Kleingrothaus, and O. Panella, *Double beta decay in left-right symmetric models*, *Phys. Lett.* **B374** (1996) 7–12, [[hep-ph/9602306](#)].
- [33] V. Tello, M. Nemevsek, F. Nesti, G. Senjanovic, and F. Vissani, *Left-Right Symmetry: from LHC to Neutrinoless Double Beta Decay*, *Phys.Rev.Lett.* **106** (2011) 151801, [[arXiv:1011.3522](#)].
- [34] J. Chakraborty, H. Z. Devi, S. Goswami, and S. Patra, *Neutrinoless double- β decay in TeV scale Left-Right symmetric models*, *JHEP* **1208** (2012) 008, [[arXiv:1204.2527](#)].
- [35] J. Barry and W. Rodejohann, *Lepton number and flavour violation in TeV-scale left-right symmetric theories with large left-right mixing*, *JHEP* **09** (2013) 153, [[arXiv:1303.6324](#)].
- [36] P. S. B. Dev, S. Goswami, M. Mitra, and W. Rodejohann, *Constraining Neutrino Mass from Neutrinoless Double Beta Decay*, *Phys.Rev.D* **88** (2013) 091301, [[arXiv:1305.0056](#)].
- [37] P. S. B. Dev, C.-H. Lee, and R. Mohapatra, *Natural TeV-Scale Left-Right Seesaw for Neutrinos and Experimental Tests*, *Phys.Rev.* **D88** (2013) 093010, [[arXiv:1309.0774](#)].
- [38] W.-C. Huang and J. Lopez-Pavon, *On neutrinoless double beta decay in the minimal left-right symmetric model*, *Eur. Phys. J.* **C74** (2014) 2853, [[arXiv:1310.0265](#)].
- [39] P. S. B. Dev, S. Goswami, and M. Mitra, *TeV Scale Left-Right Symmetry and Large Mixing Effects in Neutrinoless Double Beta Decay*, *Phys. Rev.* **D91** (2015), no. 11 113004, [[arXiv:1405.1399](#)].
- [40] D. Borah and A. Dasgupta, *Neutrinoless Double Beta Decay in Type I+II Seesaw Models*, [arXiv:1509.01800](#).
- [41] S.-F. Ge, M. Lindner, and S. Patra, *New physics effects on neutrinoless double beta decay from right-handed current*, *JHEP* **10** (2015) 077, [[arXiv:1508.07286](#)].

- [42] R. L. Awasthi, P. S. B. Dev, and M. Mitra, *Implications of the Diboson Excess for Neutrinoless Double Beta Decay and Lepton Flavor Violation in TeV Scale Left Right Symmetric Model*, [arXiv:1509.05387](#).
- [43] Riazuddin, R. E. Marshak, and R. N. Mohapatra, *Majorana Neutrinos and Low-energy Tests of Electroweak Models*, *Phys. Rev.* **D24** (1981) 1310–1317.
- [44] P. B. Pal, *Constraints on a Muon - Neutrino Mass Around 100-keV*, *Nucl. Phys.* **B227** (1983) 237.
- [45] R. N. Mohapatra, *Rare decays of the tau lepton as a probe of the left-right symmetric theories of weak interactions*, *Phys. Rev.* **D46** (1992) 2990–2995.
- [46] V. Cirigliano, A. Kurylov, M. J. Ramsey-Musolf, and P. Vogel, *Lepton flavor violation without supersymmetry*, *Phys. Rev.* **D70** (2004) 075007, [[hep-ph/0404233](#)].
- [47] B. Bajc, M. Nemevsek, and G. Senjanovic, *Probing leptonic CP phases in LFV processes*, *Phys. Lett.* **B684** (2010) 231–235, [[arXiv:0911.1323](#)].
- [48] K. Bora and G. Ghosh, *Charged lepton flavor violation $\mu \rightarrow e\gamma$ in $\mu - \tau$ symmetric SUSY $SO(10)$ mSUGRA, NUHM, NUGM, and NUSM theories and LHC*, *Eur. Phys. J.* **C75** (2015), no. 9 428, [[arXiv:1410.1265](#)].
- [49] J. C. Vasquez, *Time-reversal symmetry violation in several Lepton-Flavor-Violating processes*, *JHEP* **09** (2015) 131, [[arXiv:1504.05220](#)].
- [50] **ATLAS** Collaboration, G. Aad et al., *Search for anomalous production of prompt same-sign lepton pairs and pair-produced doubly charged Higgs bosons with $\sqrt{s} = 8$ TeV pp collisions using the ATLAS detector*, *JHEP* **03** (2015) 041, [[arXiv:1412.0237](#)].
- [51] **CMS** Collaboration, V. Khachatryan et al., *Search for heavy neutrinos and W bosons with right-handed couplings in proton-proton collisions at $\sqrt{s} = 8$ TeV*, *Eur. Phys. J.* **C74** (2014), no. 11 3149, [[arXiv:1407.3683](#)].
- [52] **ATLAS** Collaboration, G. Aad et al., *Search for heavy Majorana neutrinos with the ATLAS detector in pp collisions at $\sqrt{s} = 8$ TeV*, *JHEP* **07** (2015) 162, [[arXiv:1506.06020](#)].
- [53] S. Patra, F. S. Queiroz, and W. Rodejohann, *Stringent Dilepton Bounds on Left-Right Models using LHC data*, *Phys. Lett.* **B752** (2016) 186–190, [[arXiv:1506.03456](#)].
- [54] A. Akeroyd and M. Aoki, *Single and pair production of doubly charged Higgs bosons at hadron colliders*, *Phys.Rev.* **D72** (2005) 035011, [[hep-ph/0506176](#)].
- [55] T. Han, B. Mukhopadhyaya, Z. Si, and K. Wang, *Pair production of doubly-charged scalars: Neutrino mass constraints and signals at the LHC*, *Phys.Rev.* **D76** (2007) 075013, [[arXiv:0706.0441](#)].
- [56] P. Fileviez Perez, T. Han, G.-y. Huang, T. Li, and K. Wang, *Neutrino Masses and the CERN LHC: Testing Type II Seesaw*, *Phys.Rev.* **D78** (2008) 015018, [[arXiv:0805.3536](#)].
- [57] A. G. Akeroyd, C.-W. Chiang, and N. Gaur, *Leptonic signatures of doubly charged Higgs boson production at the LHC*, *JHEP* **11** (2010) 005, [[arXiv:1009.2780](#)].
- [58] A. Alloul, M. Frank, B. Fuks, and M. R. de Traubenberg, *Doubly-charged particles at the Large Hadron Collider*, *Phys. Rev.* **D88** (2013) 075004, [[arXiv:1307.1711](#)].
- [59] F. del Aguila and M. Chala, *LHC bounds on Lepton Number Violation mediated by doubly and singly-charged scalars*, *JHEP* **03** (2014) 027, [[arXiv:1311.1510](#)].

- [60] G. Bambhaniya, J. Chakraborty, J. Gluza, M. Kordiaczyska, and R. Szafron, *Left-Right Symmetry and the Charged Higgs Bosons at the LHC*, *JHEP* **05** (2014) 033, [[arXiv:1311.4144](#)].
- [61] B. Dutta, R. Eusebi, Y. Gao, T. Ghosh, and T. Kamon, *Exploring the Doubly Charged Higgs of the Left-Right Symmetric Model using Vector Boson Fusion-like Events at the LHC*, *Phys.Rev.* **D90** (2014) 055015, [[arXiv:1404.0685](#)].
- [62] G. Bambhaniya, J. Chakraborty, J. Gluza, T. Jeliski, and M. Kordiaczynska, *Lowest limits on the doubly charged Higgs boson masses in the minimal left-right symmetric model*, *Phys. Rev.* **D90** (2014), no. 9 095003, [[arXiv:1408.0774](#)].
- [63] A. Maiezza, M. Nemevek, and F. Nesti, *Lepton Number Violation in Higgs Decay at LHC*, *Phys. Rev. Lett.* **115** (2015) 081802, [[arXiv:1503.06834](#)].
- [64] G. Bambhaniya, J. Chakraborty, J. Gluza, T. Jelinski, and R. Szafron, *Search for doubly charged Higgs bosons through vector boson fusion at the LHC and beyond*, *Phys. Rev.* **D92** (2015), no. 1 015016, [[arXiv:1504.03999](#)].
- [65] G. Beall, M. Bander, and A. Soni, *Constraint on the Mass Scale of a Left-Right Symmetric Electroweak Theory from the $K(L) K(S)$ Mass Difference*, *Phys. Rev. Lett.* **48** (1982) 848.
- [66] Y. Zhang, H. An, X. Ji, and R. N. Mohapatra, *General CP Violation in Minimal Left-Right Symmetric Model and Constraints on the Right-Handed Scale*, *Nucl. Phys.* **B802** (2008) 247–279, [[arXiv:0712.4218](#)].
- [67] A. Maiezza, M. Nemevek, F. Nesti, and G. Senjanovic, *Left-Right Symmetry at LHC*, *Phys.Rev.* **D82** (2010) 055022, [[arXiv:1005.5160](#)].
- [68] S. Bertolini, A. Maiezza, and F. Nesti, *Present and Future K and B Meson Mixing Constraints on TeV Scale Left-Right Symmetry*, *Phys.Rev.* **D89** (2014), no. 9 095028, [[arXiv:1403.7112](#)].
- [69] S. Pascoli, M. Mitra, and S. Wong, *Effect of cancellation in neutrinoless double beta decay*, *Phys. Rev.* **D90** (2014), no. 9 093005, [[arXiv:1310.6218](#)].
- [70] C. Hagedorn, A. Meroni, and E. Molinaro, *Lepton mixing from $\Delta(3n^2)$ and $\Delta(6n^2)$ and CP*, *Nucl. Phys.* **B891** (2015) 499–557, [[arXiv:1408.7118](#)].
- [71] P. S. B. Dev, R. N. Mohapatra, and Y. Zhang, *Probing the Higgs Sector of the Minimal Left-Right Symmetric Model at Future Hadron Colliders*, [arXiv:1602.05947](#).
- [72] **SINDRUM** Collaboration, U. Bellgardt et al., *Search for the Decay $\mu^+ \rightarrow e + e + e^-$* , *Nucl. Phys.* **B299** (1988) 1.
- [73] **MEG** Collaboration, J. Adam et al., *New constraint on the existence of the $\mu^+ \rightarrow e^+ \gamma$ decay*, *Phys.Rev.Lett.* **110** (2013), no. 20 201801, [[arXiv:1303.0754](#)].
- [74] A. M. Baldini et al., *MEG Upgrade Proposal*, [arXiv:1301.7225](#).
- [75] Y. Kuno, *PRISM/PRIME*, *Nucl. Phys. Proc. Suppl.* **149** (2005) 376–378.
- [76] A. Blondel et al., *Research Proposal for an Experiment to Search for the Decay $\mu \rightarrow eee$* , [arXiv:1301.6113](#).
- [77] G. K. Leontaris, K. Tamvakis, and J. D. Vergados, *Lepton and Family Number Violation From Exotic Scalars*, *Phys. Lett.* **B162** (1985) 153.
- [78] M. L. Swartz, *Limits on Doubly Charged Higgs Bosons and Lepton Flavor Violation*, *Phys. Rev.* **D40** (1989) 1521.

- [79] V. Cirigliano, A. Kurylov, M. J. Ramsey-Musolf, and P. Vogel, *Neutrinoless double beta decay and lepton flavor violation*, *Phys. Rev. Lett.* **93** (2004) 231802, [[hep-ph/0406199](#)].
- [80] A. Ilakovac and A. Pilaftsis, *Flavor violating charged lepton decays in seesaw-type models*, *Nucl.Phys.* **B437** (1995) 491, [[hep-ph/9403398](#)].
- [81] D. Forero, M. Tortola, and J. Valle, *Neutrino oscillations refitted*, *Phys. Rev.* **D90** (2014), no. 9 093006, [[arXiv:1405.7540](#)].
- [82] **Planck** Collaboration, P. A. R. Ade et al., *Planck 2015 results. XIII. Cosmological parameters*, [arXiv:1502.01589](#).
- [83] A. Meroni, S. T. Petcov, and F. Simkovic, *Multiple CP Non-conserving Mechanisms of $\beta\beta$ -Decay and Nuclei with Largely Different Nuclear Matrix Elements*, *JHEP* **02** (2013) 025, [[arXiv:1212.1331](#)].
- [84] **GERDA** Collaboration, M. Agostini et al., *Results on Neutrinoless Double- β Decay of ^{76}Ge from Phase I of the GERDA Experiment*, *Phys. Rev. Lett.* **111** (2013), no. 12 122503, [[arXiv:1307.4720](#)].
- [85] **GERDA** Collaboration, B. Majorovits, *The search for $0\nu\beta\beta$ decay with the GERDA experiment: Status and prospects*, *AIP Conf. Proc.* **1672** (2015) 110003, [[arXiv:1506.00415](#)].
- [86] **Majorana** Collaboration, N. Abgrall et al., *The Majorana Demonstrator Neutrinoless Double-Beta Decay Experiment*, *Adv. High Energy Phys.* **2014** (2014) 365432, [[arXiv:1308.1633](#)].
- [87] R. N. Mohapatra, *Limits on the Mass of the Right-handed Majorana Neutrino*, *Phys. Rev.* **D34** (1986) 909.
- [88] A. Maiezza, M. Nemevsek, and F. Nesti, *Perturbativity and mass scales of Left-Right Higgs bosons*, [arXiv:1603.00360](#).
- [89] **ATLAS** Collaboration, G. Aad et al., *Search for high-mass diboson resonances with boson-tagged jets in proton-proton collisions at $\sqrt{s} = 8$ TeV with the ATLAS detector*, [arXiv:1506.00962](#).
- [90] **ATLAS** Collaboration, G. Aad et al., *Combination of searches for WW, WZ, and ZZ resonances in pp collisions at $\sqrt{s} = 8$ TeV with the ATLAS detector*, [arXiv:1512.05099](#).
- [91] **ATLAS** Collaboration, *Search for resonances with boson-tagged jets in 3.2 fb^{-1} of p p collisions at $\sqrt{s} = 13$ TeV collected with the ATLAS detector*, Tech. Rep. ATLAS-CONF-2015-073, 2015.
- [92] **CMS** Collaboration, *Search for massive resonances decaying into pairs of boosted W and Z bosons at $\sqrt{s} = 13$ TeV*, Tech. Rep. CMS-PAS-EXO-15-002, 2015.
- [93] J. Hisano, N. Nagata, and Y. Omura, *Interpretations of the ATLAS Diboson Resonances*, *Phys. Rev.* **D92** (2015), no. 5 055001, [[arXiv:1506.03931](#)].
- [94] K. Cheung, W.-Y. Keung, P.-Y. Tseng, and T.-C. Yuan, *Interpretations of the ATLAS Diboson Anomaly*, *Phys. Lett.* **B751** (2015) 188–194, [[arXiv:1506.06064](#)].
- [95] B. A. Dobrescu and Z. Liu, *A W' boson near 2 TeV: predictions for Run 2 of the LHC*, *Phys. Rev. Lett.* **115** (2015), no. 21 211802, [[arXiv:1506.06736](#)].
- [96] Y. Gao, T. Ghosh, K. Sinha, and J.-H. Yu, *$SU(2)SU(2)U(1)$ interpretations of the diboson and Wh excesses*, *Phys. Rev.* **D92** (2015), no. 5 055030, [[arXiv:1506.07511](#)].

- [97] J. Brehmer, J. Hewett, J. Kopp, T. Rizzo, and J. Tattersall, *Symmetry Restored in Dibosons at the LHC?*, *JHEP* **10** (2015) 182, [[arXiv:1507.00013](#)].
- [98] Q.-H. Cao, B. Yan, and D.-M. Zhang, *Simple non-Abelian extensions of the standard model gauge group and the diboson excesses at the LHC*, *Phys. Rev.* **D92** (2015), no. 9 095025, [[arXiv:1507.00268](#)].
- [99] P. S. B. Dev and R. N. Mohapatra, *Unified explanation of the $eejj$, diboson and dijet resonances at the LHC*, *Phys. Rev. Lett.* **115** (2015), no. 18 181803, [[arXiv:1508.02277](#)].
- [100] F. F. Deppisch, L. Graf, S. Kulkarni, S. Patra, W. Rodejohann, N. Sahu, and U. Sarkar, *Reconciling the 2 TeV Excesses at the LHC in a Linear Seesaw Left-Right Model*, [arXiv:1508.05940](#).